

1 A new approach to mapping landslide hazards: a
2 probabilistic integration of empirical and
3 ~~process-based~~physically-based models in the
4 North Cascades of Washington, U.S.A.

5
6
7 Ronda Strauch¹, Erkan Istanbulluoglu², and Jon Riedel³
8

9 1. Seattle City Light, Seattle, WA and Civil and Environmental Engineering, University of
10 Washington, Seattle, WA

11 2. Civil and Environmental Engineering, University of Washington, Seattle, WA

12 3. National Park Service, US Dept. of Interior, Sedro-Woolley, WA

13
14 Corresponding author:

15 Ronda Strauch
16 Seattle City Light
17 700 5th Ave #3316, Seattle, WA 98124
18 Tel: 425-445-7934
19 E-mail: ronda.strauch@seattle.gov

20
21 **Keywords:**

22 Landslide, frequency ratio, hazard, North Cascades, geomorphology, debris avalanche

24 **Abstract**

25
26 We developed a new approach for mapping landslide hazard by combining probabilities of
27 landslide impact derived from a data-driven statistical approach and ~~process-based~~physically-
28 based model of shallow landsliding. Our statistical approach integrates the influence of seven site
29 attributes on observed landslides using a frequency ratio method. Influential attributes and
30 resulting susceptibility maps depend on the observations of landslides considered: all types of
31 landslides, debris avalanches only, or source areas of debris avalanches. These observational
32 datasets reflect the capture-detection of different landslide processes or components, which relate
33 to different landslide-inducing factors. For each landslide dataset, a Stability Index (SI) is
34 calculated as a multiplicative result of the frequency ratios for all attributes and is mapped across
35 our study domain in the North Cascades National Park Complex, Washington, U.S.A. A

continuous function is developed to relate local SI values to landslide probability based on a ratio of landslide and non-landslide grid cells. Slopes greater than 35° are more frequently associated with landslide initiation, while higher landslide hazards at gentler slopes (<30°) reflect depositional processes from observations of all landslide types or debris avalanches. Source areas are associated with mid to high elevations (1,400 to 1,800 m), where they are linked to ecosystem transition (e.g., forest to barren), while all landslide types and debris avalanches show increasing frequency in lower elevations (<1,200 m). Slope is a key attribute in the initiation of landslides, while lithology is mainly linked to transport and depositional processes. East (west) aspect is a positive (negative) landslide influencing factor, likely due to differences in forest cover and associated root cohesion, and evapotranspiration. The empirical model probability derived from the debris avalanche source area dataset is combined probabilistically with a previously developed process-based physically-based probabilistic model. A two-dimensional binning method employs empirical and physically-based probabilities as indices and calculates a joint probability of landsliding at the intersections of probability bins. A ratio of the joint probability and the physically-based model bin probability is used as a weight to adjust the original physically-based probability at each grid cell given empirical evidence, to produce an integrated probability of landslide initiation hazard for initiation that includes mechanisms not captured by the infinite slope stability model alone. Improvements in distinguishing potentially unstable areas with the proposed integrated model are statistically quantified. We apply our approach in North Cascades National Park Complex in Washington, USA, to provide multiple landslide hazard maps that land managers can use for planning and decision making, as well as for educating the public about hazards from landslides in this remote high-relief terrain.

1 **1 Introduction**

2 Most mountain ranges are susceptible to landsliding due to their steep geomorphology, loose soil
3 development, geology, and high precipitation (e.g., Coe, 2016). Landslides disrupt aquatic
4 habitats (May et al., 2009; Pollock, 1998), damage infrastructure such as roads, utilities, and
5 dams (Ghirotti, 2012; Baum et al., 2008), and harm people (Wartman et al., 2016; Taylor and
6 Brabb, 1986). Landslide hazards are expected to increase globally with growing extremes in the
7 climate (Coe, 2016; Haeberli et al., 2016; Crozier 2010).

8 Maps of landslide hazards, quantified as a probability of landslide initiation or impact, can be
9 obtained using empirical methods that statistically relate the location of existing landslides to
10 other environmental variables and process-based physically-based models based on geotechnical
11 slope stability equations driven by hydro-climatic inputs (Bordoni et al., 2015; Mancini et al.,
12 2010; Sidle and Ochiai 2006; El-Ramly, et al., 2002). While detailed quantitative and categorical
13 climatic, geologic, ecologic, and pedologic information can be used in statistical models,
14 process-based physically-based models are limited to geotechnical stability analysis driven by
15 soil pore-water pressure, and often neglect geological factors such as bedrock, faulting, and
16 complexities of microclimatic conditions. To date, data-driven empirical research on landslide
17 hazard mapping (Corominas et al., 2012; Lee 2007; Chung and Fabbri 2002) has been typically
18 conducted independently from hydroclimate-driven modeling of landslides that largely focus on
19 hydrologic controls on landsliding (Wooten et al., 2016; Cevasco et al., 2014). There is need for
20 unifying these two lines of research to provide regional scale landslide prediction for resource
21

1 management and hazard mitigation strategies. In this paper we develop a statistical approach to
2 combine probability of landslide initiation obtained from an observation-based statistical
3 mapping method and a process-basedphysically-based model. The proposed approach is
4 illustrated in the North Cascades region of the state of Washington, USA.

5
6 Data-driven statistical landslide susceptibility approaches assess the inherent or quasi-static
7 stability of hillslopes derived from statistical associations (e.g., correlations) between site
8 attributes (e.g., soil, geology, topography) and an inventory of past landslides that includes
9 landslide type and locations (e.g., Dai and Lee, 2002; Gupta and Joshi, 1990; Pachauri and Pant,
10 1992; Kirschbaum et al., 2012). These models focus on prevailing conditions that predispose
11 hillslopes to failure (Hung et al., 2014), typically providing general indices of relative landslide
12 susceptibility or spatial probabilities applicable to the study location and cannot represent causal
13 factors or triggering conditions that change in time (van Westen et al., 2006; Sidle and Ochiai,
14 2006). Outcome of such analyses depend on the completeness of observations, hindering the use
15 of such techniques over large areas where complete inventories are typically lacking. Since
16 empirical models are based on observation of past landslides, the preconditioning relationships
17 are assumed to prevail into the future until an updated study is completed (Lepore et al., 2012).

18
19 Process-basedPhysically-based models require considerable data on the spatial-temporal
20 characteristics of the landscape and triggering hydro-meteorologic events. These models are also
21 usually restricted to a specific type of landslide and can be limited in representing local geologic,
22 soil, and hydrologic conditions that may be difficult to observe and map in the field and
23 parameterize in model theory. Data-driven statistical methods could be used to condition
24 process-basedphysically-based model results to incorporate the influence of environmental and
25 geologic factors that are not represented in process theory. Linking these empirically-based and
26 process-basedphysically-based models may improve the spatial-temporal patterns of landslide
27 hazard at medium to large scales where landslide inventories exist to provide support tools for
28 authorities addressing risk management. Additional descriptions of the advantages and
29 disadvantages of data-driven and physically-based models and landslide hazards assessments can
30 be found in reviews by Ercanoglu and Sonmez (2019), Reichenback, et al. (2018), Hung (2018),
31 and Aleotti and Chowdhury (1999).

32
33
34
35 This paper describes research designed to address the following questions: 1) How can we
36 quantify relative contributions of local topography, geology, and ecology on landslide frequency
37 and derive spatial probabilities of landsliding using a statistical model? 2) How would
38 probabilities of landslide initiation derived from empirical observations compare with those
39 derived from a process-basedphysically-based model? 3) How can we combine empirical and
40 process-basedphysically-based models for landslide susceptibility to improve the prediction of
41 landslide hazards?

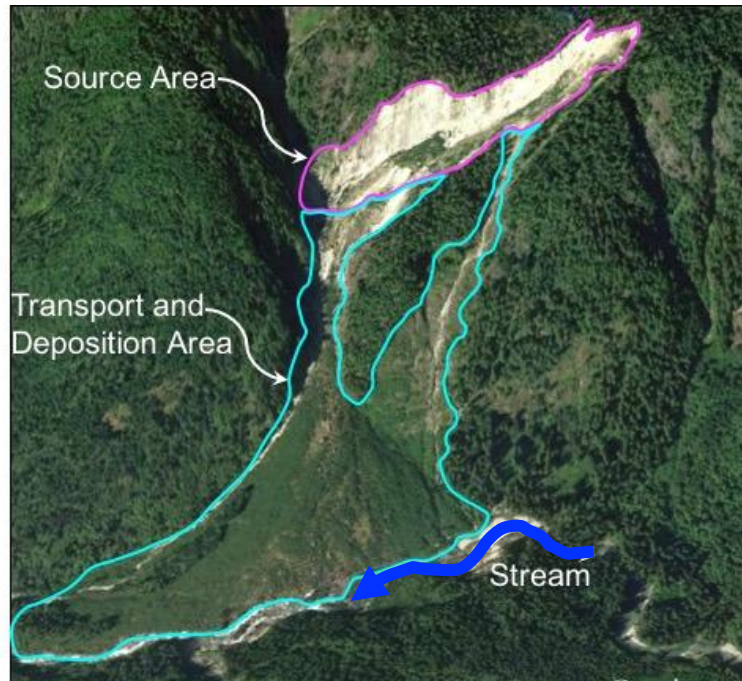
42
43 The empirical approach for landslide susceptibility we used is based on a modification of the
44 Frequency Ratio (FR) statistical concept which has been found to perform as well as more
45 rigorous statistical approaches such as logistic regression (Hong et al., 2017; Wu et al., 2017;

1 Bellugi et al., 2015; Lepore et al., 2012; Kirschbaum et al., 2012; Lee and Pradhan, 2007; Lee et
2 al., 2007). As for the mechanistic model, we used the results of Strauch et al. (2018), who
3 developed a Monte Carlo solution of the infinite slope stability equation coupled to a steady-state
4 topographic flow routing approach to map annual probability of shallow landsliding. The
5 uncertainty of soil depth in Strauch et al. (2018) was constrained by a soil development model,
6 and subsurface flow recharge was obtained from a regional macro-scale hydrologic model that
7 produced historical hydrologic simulations (Hamlet et al., 2013).

8
9 Building on the advantages from the empirical and process models, we combined the two models
10 to develop a map of landslide hazard. The integrated map can be developed to identify landslide
11 hazards that may originate from ~~either~~ the initiation of landslides and used to inform models of
12 or the transport and deposition (i.e., runout) of ~~the~~ landslide material (Fig. 1). The focus of the
13 study was to determine if an empirical-based model of landslide hazard could be used to improve
14 an existing physically-based model for shallow landslide probability. The organization of this
15 paper is as follows. Our methodology is discussed in Sect. 2, including the empirical method,
16 model application, data compilation, and model integration approach. Sect~~ion~~ 3 details our
17 results of the empirical application and integrated hazard model as well as various hazard maps
18 developed. We end with some overall concluding thoughts in Sect. 4.

19

1



2



3 **Figure 1.** Primary landslide features [of the Goodell Creek landslide \(Oct. 2003\)](#) showing source,
4 transport, and deposition areas illustrated over aerial image from Google Earth [taken July 2016](#). [Base of](#)
5 [landslide is about 1 km across](#). Location in North Cascades National Park Complex about 4 km north of
6 Newhalem, Washington. Source: Google Earth, $48^{\circ}41'55.72''$ N $121^{\circ}17'01.31''$ W, imagery data [June 23,](#)
7 [2006 viewed towards southwest](#). [12/30/2010](#).

8

2 Methodology

2.1 Frequency Ratio

We characterized the susceptibility of hillslopes to landslides using an empirically-based Frequency Ratio, FR, approach (Lee et al., 2007; Kirschbaum et al., 2012). We used the term landslides broadly, covering all types of mapped landslides in our landslide inventory, with their source, transport and depositional zones (Fig. 1). The FR approach relates the density ratio of historical landslides within selected surface attributes, SAs. We considered seven SAs in our analysis: slope, elevation, aspect, curvature, land use-land cover (landcover), lithology, and topographic wetness index.

Slope, curvature, and lithology directly affect the forces and geotechnical properties in surface sediments. Land cover provides a surrogate for root cohesion and topographic wetness index has been used as a surrogate for soil pore water pressure (Borga et al., 2002). Elevation can represent the effects of climate, weathering, vegetation, ground motion, and glacial processes, if any, as well as coincide with variability in slope, soil depth, and land use (Sidle and Ochiai, 2006). Aspect provides an indication of solar insolation, vegetation type and cover density, snow and ice loading, and soil moisture levels via evapotranspiration (Beaty, 1956; Gokceoglu et al., 2005).

Each SA is indexed by attribute type, m (e.g. m =slope, lithology, vegetation), and its subcategory is indexed by n . Subcategories of each SA can be a categorical variable such as type of lithology, soil and vegetation, or a quantitative variable defined with certain ranges such as slope and aspect over the study domain, SD. For a given SA, identified by m , and its subcategory, n , $FR_{m,n}|SA_{m,n}$ is calculated (Eq. 1) as the ratio of observed landslide area, LA, in each SA m and subcategory n ($LA_{SA_{m,n}}$) with respect to the area of the SA $_{m,n}$ ($A_{SA_{m,n}}$) to the regional landslide density, P_o (Eq. 2) (Miller and Burnett, 2007):

$$FR_{m,n}|SA_{m,n} = \frac{LA_{SA_{m,n}}/A_{SA_{m,n}}}{P_o} \quad (1)$$

$$\text{where } P_o = \frac{LA_{SD}}{A_{SD}} \quad (2)$$

The term in the numerator of Eq. (1) gives an empirical probability of landsliding impact within $SA_{m,n}$. P_o can also be referred to as a regional background probability, such that in absence of any other information, P_o represents the probability of landsliding at any point in the domain. The interpretation of FR is as follows (Lepore et al., 2012):

- $FR < 1$: indicates proportionally less landslide area with subcategory n of SA m , $SA_{m,n}$; hence, smaller odds of a landslide than in the entire SD.
- $FR = 1$: means there is the same proportion of landslide area with $SA_{m,n}$ as in the SD thus, the odds of a landslide are the same for the $SA_{m,n}$ subcategory as the SD.
- $FR > 1$: reveals a higher percentage of landslide area with $SA_{m,n}$, than in the entire SD, so there is a propensity for failures to occur with this SA.

FR in Eq. (1) is developed for a population of spatially distributed locations that has the same attribute of a given $SA_{m,n}$. A given point on the landscape would have as many FR values as the number of SAs used. To develop an index that will incorporate all the FR values for a given

1 point on the landscape we used an empirical susceptibility index, SI, defined at the grid cell
2 scale, SI_c , as the product of the FR values for all SAs of that grid cell and their associated
3 subcategory,

4

$$5 \quad SI_c = \prod^m FR_{m,n} | SA_{m,n}. \quad (3)$$

6

7 A multiplicative FR is used because in certain subcategories, there may be no landslide
8 observations (e.g., low slope angle), and in such cases the hillslope would be stable regardless of
9 other soil and vegetation properties. SI_c is a measure that relates local static (or slowly changing)
10 site characteristics to relative frequency of landslides. Since SI_c is a data-driven index,
11 probability of landsliding would increase as SI grows.

12

13 In order to develop a continuous relationship between SI_c and probability of landslide at a grid
14 cell, $P(LS_c|SI_c)$, we binned the population of SI_c values across the landscape into SI_r bins, where r
15 is the number of SI bins. We then estimated the probability of landsliding for an SI bin, SI_r ,
16 $P(LS_r|SI_r)$, as the ratio of number of grid cells with landslides in each SI bin, $N(LS)_r$, to the total
17 number of grid cells within each SI bin, N_r (Eq. 4).

18

$$19 \quad P(LS_r|SI_r) = \frac{N(LS)_r}{N_r} \quad (4)$$

20

21 To calculate spatially continuous empirical probability of landsliding at each grid cell of a DEM,
22 $P(LS_c|SI_c)$, we fit empirical functions that relate $P(LS_r|SI_r)$ to SI_r . These functions are then used
23 for mapping empirical probability of landsliding at the cell scale, $P(LS_c|SI_c)$, based on its
24 empirically-derived SI_c value in Eq. (3).

25

26 We included all SAs to develop empirical models relating SI to landslide probability, similar to
27 Kirschbaum et al. (2012) and Lepore et al. (2012). We repeated the analysis described above
28 three times: first, considering all landslide types and including their source, transport, and
29 depositional zones, as is commonly done in multi-factor analyses (Sidle and Ochiai, 2006;
30 Ayalew et al., 2004; Carrara et al., 1995); second, focusing on debris avalanches, with all three
31 of their zones (Fig. 1); and third, considering only the source (initiation) areas of debris
32 avalanches. These source areas were identified as the upper 20% of by elevation within mapped
33 debris avalanche polygons. which appeared to align with inspections of aerial imagery of a
34 selected debris avalanches. This tiered approach can be used to quantify the relative
35 contributions of different landslide features to overall landslide hazard in a region as well as
36 inform the variability in hazard identification given a landslide dataset.

37

38 2.2 Model Integration

39 Here we develop a method to combine the empirical probability for landslide initiation based on
40 SI, $P(LS_c|SI_c)$, with the probability of landslide initiation based on a previously developed
41 physically-based model using Landlab (Strauch et al., 2018; Hobley et al., 2017). The physically-
42 based model employs Monte Carlo solution of the infinite slope stability model that evaluates
43 localized (model grid cell) factor of safety (FS), and calculates the annual probability of failure at
44 a cell, $P(FS_c \leq 1)$ as the number of Monte Carlo iterations where probability of failure ≤ 1 out

1 ~~of divided by the total number of iterations, using Landlab (Strauch et al., 2018; Hobley et al.,~~
 2 ~~2017). Precipitation is considered in the physically-based model through its use as input to a~~
 3 ~~macro-scale hydrology model, such as the Variable Infiltration Capacity model (Liang et al.~~
 4 ~~1994), which produces a spatially distributed recharge field used to represent steady-state~~
 5 ~~drive the steady-state subsurface flow in the stability model in the component. Other hydro-~~
 6 ~~geophysical stochastic inputs into the stability model are selected from distributions while slope~~
 7 ~~and specific contributing area are deterministic variables.~~

8
 9 In combining probabilities, we focus on the landslide *initiation* areas, as the ~~process-~~
 10 ~~basedphysically-based~~ model we used would only be applicable for landslide initiation.
 11 Empirical $P(LS_c|SI_c)$ and modeled $P(FS_c \leq 1)$ probabilities of landslide impact at each cell defined
 12 across the landscape are treated as indices representing the likelihood of landslides. The method
 13 we proposed for an integrated probability uses the cell count of observed landslide initiation
 14 points within bins of the empirical, $P(LS_c|SI_c)_b$, and modeled probability, $P(FS_c \leq 1)_b$ of
 15 landsliding.

16
 17 If we treat the empirical probability as an index, the probability of landslide initiation within a
 18 bin j of empirically-derived probability of landslide initiation, $E_j = P(LS_c|SI_c)_{b,j}$ is calculated as:

$$19 P(LS|E_j) = \frac{N(LS)_j}{N_j} \quad (5)$$

20 where, $N(LS)_j$ is the number grid cells with observed landslides and N_j is the number of grid
 21 cells both in bin j of E_j :

22
 23 Similarly, the probability of landslide initiation within a bin i of ~~processed-basedphysically-~~
 24 ~~based~~ modeled probability of landslide initiation, $M_i = P(FS_c \leq 1)_{b,i}$ is calculated as:

$$25 P(LS|M_i) = \frac{N(LS)_i}{N_i} \quad (6)$$

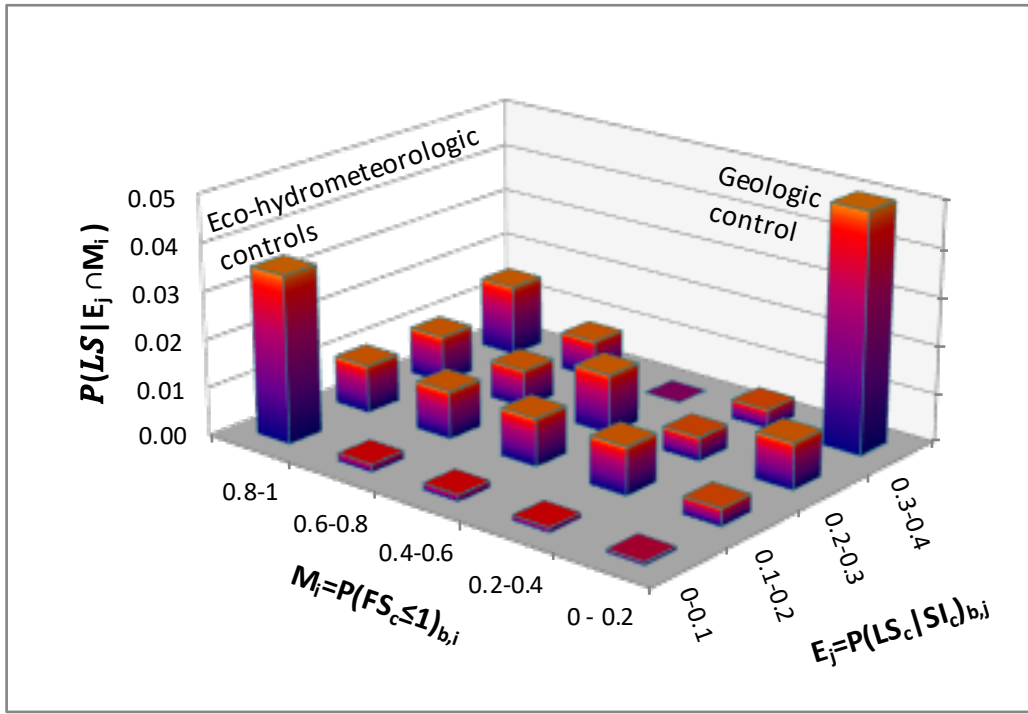
26 where, $N(LS)_i$ is the number of grid cells with observed landslides and N_i is the number of grid
 27 cells both in bin i of M_i . If the observed landslide data is representative of the actual landslide
 28 frequency over the duration when the probability of landsliding is modeled, an ideal model that
 29 correctly represents all environmental variables associated with landslide initiation would give
 30 $P(LS|M_i) = M_i$. Assuming unbiased landslide mapping in the field, a greater difference
 31 between these two relative frequency probabilities would suggest a weaker model representation
 32 of the process, especially when the ~~process-basedphysically-based~~ model is run to represent
 33 landslide risk for a given climatology.

34
 35 Modeled probabilities may be improved when information contained in empirical probabilities is
 36 introduced. The probability of landslide initiation in areas shared by any two select bins (e.g., co-
 37 bins) of empirically-derived, E_j , and ~~process-basedphysically-based~~ modeled, M_j , probabilities is
 38 calculated as the joint probability:

$$39 P(LS|E_j \cap M_i) = \frac{N(LS)_{j,i}}{N_{j,i}} \quad (7)$$

1 where $N(LS)_{j,i}$ is the number grid cells with observed landslides and $N_{j,i}$ is the number of grid
 2 cells in the *joint* bin j of empirical probability and bin i of modeled probability data. An
 3 illustration of this estimation is given in Figure 2. The conceptual example shows how relatively
 4 low landslide probability predictions by a process model in the $M_i=0-0.2$ bin range can be
 5 modified due to differences in the empirical preconditioning of the landscape (e.g., rock type) to
 6 landslides represented in E_j . The intersection of $M_i=0-0.2$ with $E_j=0.2-0.3$ yields a higher
 7 empirical probability of landsliding. Influence of vegetation change and extreme weather events
 8 (e.g. Eco-hydrometeorologic controls) that were not part of the initial empirical data set used for
 9 estimating E_j bins can be captured by the [process-based physically-based](#) model. In this case the
 10 model predicts a high probability $M_j=0.8-1$, while E_i remained in the low probability range in
 11 $E_i=0.0-0.1$. The intersection of M_j and E_i land surface characterization captures the landscape
 12 where landslides were observed.

13
 14
 15



16
 17

18 **Figure 2.** Illustration of the proposed landslide probability conditioned on estimated spatially distributed
 19 empirical and modeled probabilities as binned indices, E_j and M_i , that form a joint space.
 20 $P(LS|E_j \cap M_i)$ is defined as the ratio of the number of landsliding cells to the number of cells that jointly
 21 fall into given E_j and M_i bins.

22

23 We propose that the ratio of $P(LS|E_j \cap M_i)$ and $P(LS|M_i)$ can be used as a correction to
 24 $P(FS_c \leq 1)$. As model predictions improve, this ratio should get closer to 1, especially when the
 25 model is used to map landslide probability for a given climatology in a region. When the
 26 [process-based physically-based](#) model is run for studying a specific rainfall event, this ratio
 27 quantifies the relative roles of other factors could play on landslide initiation. Thus, we propose

1 that the probability of landsliding at each grid cell, c , given the corresponding M_j and E_i bins that
 2 a cell belongs to can be estimated as:

$$3 P(LS)_{c,j,i} = P(FS_c \leq 1) \times \frac{P(LS|E_j \cap M_i)}{P(LS|M_i)} \quad (8)$$

4 If we let ω represent the bin-based ratio on the right-hand side of Eq. (8) as a weighting factor
 5 based on observations of landslides, then we can simplify notation to:

$$6 P(LS)_{c,j,i} = P(FS_c \leq 1) \times \omega \quad (9)$$

7
 8 This gives the probability of landslide initiation, represented as an *adjusted* modeled probability
 9 of landslide initiation at a grid cell given empirical observations correlated with site
 10 characteristics. In the remainder of the paper we use $P(FS_c \leq 1)$ to refer to process-based
 11 physically-based shallow landslide probability from Strauch et al.(2018) and $P(LS)$ to refer
 12 to the adjusted model probability using the proposed empirical-adjustment methodology.

13 A hypothetical example shown in Table 1 demonstrates calculating the relative frequencies, the
 14 resulting calculated weight, and adjusted $P(LS)$ (Eq. 9). The calculation of relative frequency is
 15 based on binning modeled and empirical probabilities, counting landslide and non-landslide cells
 16 within each bin, and calculating a weighting term, ω , which is then used to adjust the original
 17 modeled probability given empirical evidence. Weights can be greater than 1 and the final
 18 probability will be increased when weight ≥ 1 and decreased when weight < 1 . Final adjusted
 19 probabilities are limited to unity in the integrated model. For example, a weight = 2 and modeled
 20 probability = 0.2 would result in a doubling of the final probability = 0.4 given empirical
 21 information.

22 **Table 1.** Hypothetical example of calculating relative frequencies, weight, and $P(LS)$ during
 23 model integration

E_j bins	Observed Landslides / Total Cell Count (<i>relative frequency</i>)					Total
0.2-0.3	206/ 870	5/ 24	3/ 14	5/ 14	2/ 10	221/ 932
0.1-0.2	11107/ 87104	309/ 2001	193/ 1220	137/ 856	96/ 657	11842/ 91838
0 - 0.1	48513/ 1848950	1757/ 51679	1157/ 33084	793/ 24928	742/ 21410	52962/ 1980051
<i>Total</i>	59826/ 1936924	2071/ 53704	1353/ 34318	935/ 25798	840/ 22077	65025/ 2072821
M_i bins	0-0.1	0.1-0.2	0.2-0.3	0.3-0.4	0.4-0.5	
An example calculation of $P(LS)$ using the above data – a cell having a modeled probability, $P(FS_c \leq 1) = 0.12$ and an empirical probability, $P(LS_c SI_c) = 0.08$, then: $P(LS E_j) = 52962/1980051 = 0.027$ (Eq. 5) $P(LS M_i) = 2071/53704 = 0.039$ (Eq. 6) $P(LS E_j \cap M_i) = 1757/51679 = 0.034$ (Eq. 7) $\omega = 0.034/0.039 = 0.87$ $P(LS)_{c,j,i} = 0.12 \times 0.87 = 0.105$ (Eq. 9)						

1
2 2.3 Model application
3

4 2.3.1 Study Area
5

6 Our study area is within the geographical limits of North Cascades National Park Complex
7 (NOCA) managed by the U.S. National Park Service (Fig. 3). NOCA has experienced damaging
8 and disruptive landslides that have impacted infrastructure and disrupted public use of the park.
9 NOCA is approximately 2,757 km², with 93% wilderness (e.g., no motorized or mechanized
10 devices) (DOI-NPS, 2012), which is ideal for studying landslides primarily triggered by natural
11 causes. The north-south oriented Cascade Mountains has an elevation range of 100 to 2,800 m at
12 the study site, with jagged bedrock peaks, and over 300 alpine glaciers. The landscape has been
13 shaped by Ice Age continental and alpine glaciers, and mass wasting, fluvial and tectonic uplift
14 processes that continue today (LaHusen et al., 2016; Mustoe and Leopold, 2014; Collins and
15 Montgomery, 2001; Riedel et al., 2007; Pelto and Riedel, 2001). The bedrock geology in the
16 park is dominated by gneiss and granite, with lower grade metamorphic rocks schist and phyllite
17 on the western edge of the park, and Mesozoic sedimentary rocks on the eastern flank (Tabor and
18 Haugerud, 1999). Placement of granite at depth along faults led to hydrothermal alteration of
19 some overlying rocks, and the clustering of large landslides. Soils in the park are generally
20 coarse-grained and relatively young due to active slope processes, but soil age, thickness and
21 distribution are highly variable. Soils formed in glacial deposits from the last glaciation are also
22 widespread, and many soils are classified based on the amount of volcanic ash they contain.

23 Orographic uplift of Pacific Ocean air masses generates a spatial precipitation gradient with an
24 average of 4,575 mm of precipitation falling annually on the highest elevations west of the crest,
25 while lowlands east of the crest receive a mean annual precipitation of 708 mm (Mustoe and
26 Leopold, 2014; Roe, 2005). Air temperatures vary highly depending on season and elevation
27 with the warmest month typically August and the coldest month is January; corresponding
28 average daily temperatures of about 25° C and 4°C, respectively, for these months in Newhalem,
Washington.

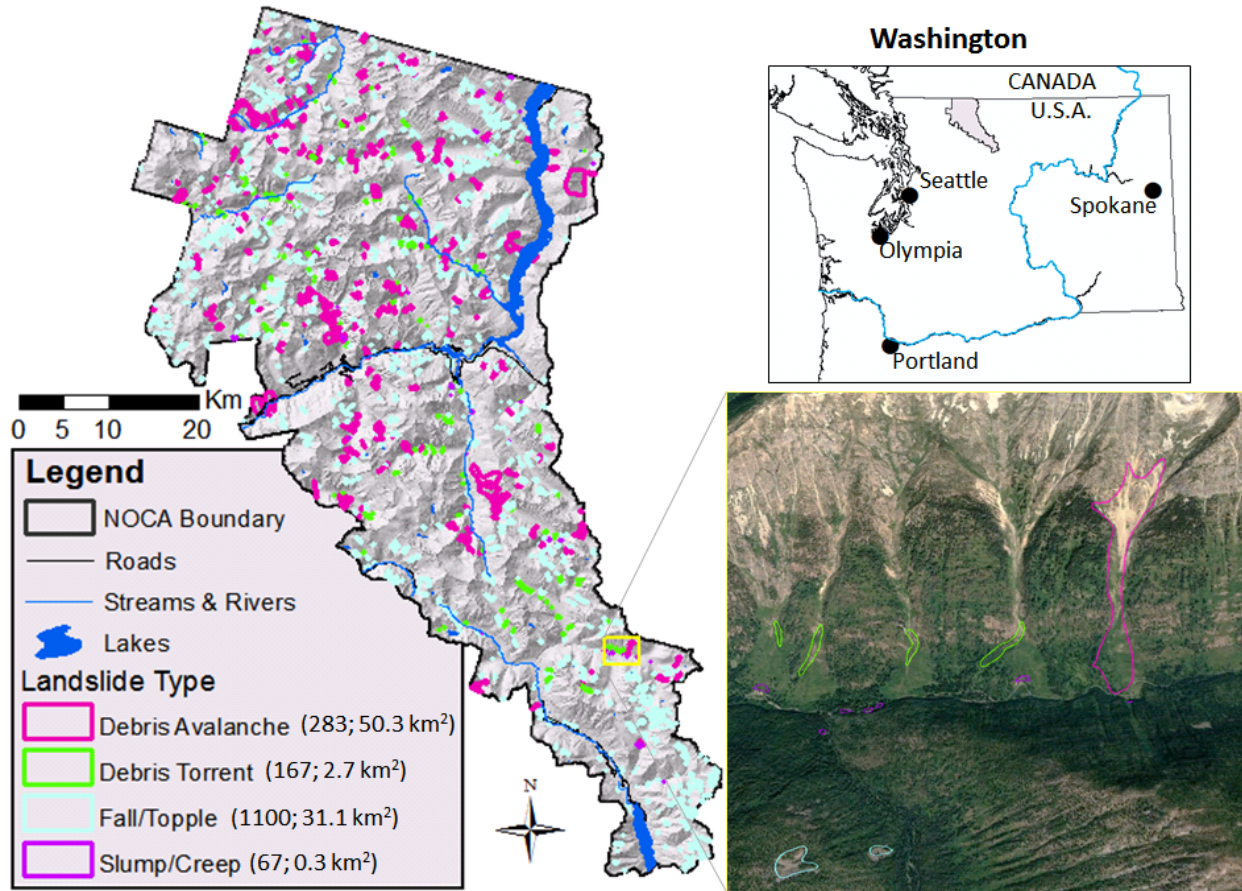


Figure 3. Four landslide types mapped within North Cascades National Park Complex (NOCA) in Washington, U.S.A. The number and their total area of each type is given in parentheses. Insert provides example of mapping over aerial image from Google Earth, 48°27'20.21" N 120°44'47.09" W, imagery data [8/27/August, 27, 2006](#).

Vegetation in NOCA is dominated by forest, particularly coniferous tree species, up to about 2,000 m (Strauch et al., 2018; Agee and Kertis, 1987). A patchwork of shrubs, herbaceous vegetation, and barren land is found above this elevation common in alpine environments and in the paths of frequent snow avalanches. Above 2,400 m is mostly bare rock, snow and ice. The underlying geology is composed of a primarily old Mesozoic crystalline and metamorphic rock originating far to the south (Haugerud and Tabor, 2009).

Landslide (LS) inventory data are the most requisite information needed for an empirical statistical analysis (Lepore et al., 2012). Landslides were mapped in the [2,768 km²](#) park as discreet landforms during a [comprehensive](#) park-wide [landslide](#) inventory (Fig. 3; Riedel and Probala, 2005). Landslides were identified using [color](#)-stereo-pair [1998](#) air photos [taken since 1960s](#) at [1:24,000 and](#) 1:12,000 scale, 7.5 minute topographic maps, bedrock geology maps, and field investigations (e.g., Riedel et al., 2012). The minimum mapping unit was approximately 1,000 m² except for some smaller slump units. Landslide linework was transferred to a digital format, peer reviewed, and polygons edited into final form in geographical information system (GIS) software using National Agriculture Imagery Program (NAIP) imagery and a 10-m DEM

1 and, in some cases, LiDAR. Where areas were mapped by traditional methods, and Lidar later
2 became available, the original approach captured most (~75%) of the landslides. Dense
3 vegetation cover and a lack of access limited identification of some existing landslides. Larger,
4 more recent debris avalanches that left large deposits on the valley floor were more easily
5 recognized and mapped. Ancient landslides that occurred before the last glacial period 16,000
6 years ago were generally not mapped because their deposits were buried or reworked by
7 subsequent continental glaciation.

8
9 The landform mapping study identified six different types of mass wasting (Table 2): rock
10 fall/topple, debris avalanche, debris torrent, slump/creep, sackung, and snow avalanche-impacted
11 landforms (SAILs) (Riedel et al., 2012). The single sackung mapped in NOCA represents a
12 gravitational spreading or slope deformation, sometimes found near ridge tops. All landslide
13 types were included in the analysis except for the rare sackung and SAILs, which are created by
14 snow avalanche impacting unconsolidated sediments rather than slope instability. The idea is to
15 capture more spatial variability and geologic controls on observed landslides by using all the data
16 we obtained for available from the inventory for the four common landslide types. There are
17 1,618 landslides mapped in NOCA: falls/topples (68%), debris avalanches (17%), debris torrents
18 (10%), slumps/creeps (4%), and one sackung (<1%) (Fig. 3; sackung not shown).
19

20 **Table 2.** Landslides mapped as part of comprehensive landform mapping study used in hazard
21 analysis (Riedel et al., 2005)

Type of Mass Wasting	Process	Mapping
Debris Avalanche	Extremely rapid moving mixture of rock, soil, and vegetation, generally originates from glacially-sourced areas, over-steepened valley walls, and in many cases hydrothermally altered bedrock	Includes headwall scar, path, and deposit
Debris Torrent	Channelized rapid and/or sudden flow of material entraining debris stored in stream channel while moving down slope	Only the deposition areas within a debris cone
Slump and Creep	Slumps - rotational slip of cohesive sediments, usually triggered by undercutting of steep slopes along riverbanks. Creeps - slow movement induced by saturated ground.	Mapped where deciduous vegetation brighter on aerial photos, fresh new soil, jackstraw or pistol gripped trees.
Rockfall or Rock Topple	Sporadic and shallow detachment of rock falling from bedrock cliffs and rock towers	Mapped where bright and highly reflective with little or no vegetation on aerial photos. Mainly deposition mapped.

1 2.3.2 Study domain and Parameters

2 We constrained our analysis to soil-mantled landscapes by excluding high elevation areas
3 covered by glaciers, permanent snowfields and exposed bedrock, as well as wetlands and other
4 water surfaces, based on landform mapping and maps of lithology and landcover. We also
5 exclude slopes less than 17° because this slope threshold was found to generally separate
6 colluvial mass wasting and debris transport processes from fluvial processes in this region
7 (Strauch et al., 2018). The area included in the analysis covers about 79% of NOCA's land area.
8

9 The seven site attributes (SAs) investigated using the Frequency Ratio (FR) approach as they
10 relate to mapped landslide activity vary across the NOCA study area. Slope, total curvature
11 (Laplacian of elevation), and aspect attributes were derived using ArcGIS from a 30-m digital
12 elevation model (DEM) acquired from National Elevation Dataset (NED) (USGS, 2014a). A
13 resolution of 30-m was chosen for comparability with other studies and landslide size (e.g.,
14 Strauch et al., 2018; Lepore et al., 2012). Elevation ranges from 107 to 2794 m with 85% of the
15 park between 500 to 2000 m. Subcategories for elevation were based on 200-m increments with
16 lumping at the ends (e.g., < 400 m and > 2200 m). Slope subcategories were set at 5° increments
17 with ending subcategories for slopes 17-25°, and >50°. Curvature was divided into three
18 subcategories: convex/diverging, flat, or concave/converging. Aspect (i.e., facing direction of
19 slope) was classified into eight compass orientations (i.e., N, NE, E, SE, S, SW, W, NW). The
20 park's complex topography results in roughly equal distribution among the cardinal and
21 intercardinal directions of aspect; however, the southwest quadrant is slightly more common.
22

23 The DEM also provides the information needed to derive a distributed wetness index (Beven and
24 Kirkby, 1979; O'Loughlin, 1986), calculated as the natural log of the ratio of specific catchment
25 area [L] to sine of local slope. This index has been used for quantifying the contribution of pore-
26 water pressure to destabilizing forces in landslide modeling (e.g., Borga et al., 2002; Gokceoglu
27 et al., 2005). Wetness index was divided into 5 subcategories based on 20% quantiles: low, low-
28 medium, medium, medium-high, and high wetness. Landcover was acquired from the 2014
29 National Land Cover Data (NLCD), which is based on 2011 Landsat satellite imagery (Jin et al.,
30 2013; USGS, 2014b). We categorized this into forest, shrubland, herbaceous, water, wetland,
31 snow/ice, barren, and developed (e.g., roads, campgrounds). Based on this classification, forest,
32 shrubs, and herbaceous vegetation represent 54%, 15%, and 10% of the park, respectively.
33 Barren and snow or ice combined cover 17%, typically at the high elevations. Water and
34 wetlands cover about 2.5%, while developed is less than 0.5%.
35

36 Lithology provides a description of rock and deposits that indicates composition, strength, and
37 age, which can influence the hillslope strength and water redistribution. Washington State
38 Department of Natural Resources (WADNR) provides lithology in its surface geology maps that
39 display rocks and deposits as geologic map units (WADNR, 2014). This source of information
40 was chosen because it is available for all of Washington, facilitating future applications. There
41 are 48 lithology map unit types within NOCA. These were aggregated into seven subcategories,
42 based on similarities in origin and generally increasing strength, called: (1) unconsolidated
43 sediment, (2) ultramafic, (3) weak metamorphic foliated, (4) sedimentary rock, (5) hard
44 metamorphic, (6) intrusive igneous, and (7) volcanic/extrusive igneous (Table 3). Water and ice
45

were not classified. Both landcover and lithology were rasterized to the same DEM grid resolution using ArcGIS based on the dominant type of attribute in each grid cell. Among the seven types of lithology, hard metamorphic is most common (41% of NOCA), while ultramafic, sedimentary rock, and volcanic/extrusive igneous combined make up less than 5%.

Table 3. Classification of Washington Department of Natural Resources surface geology from generally weaker (1) to stronger (7) material along with aerial percentages within NOCA in parentheses

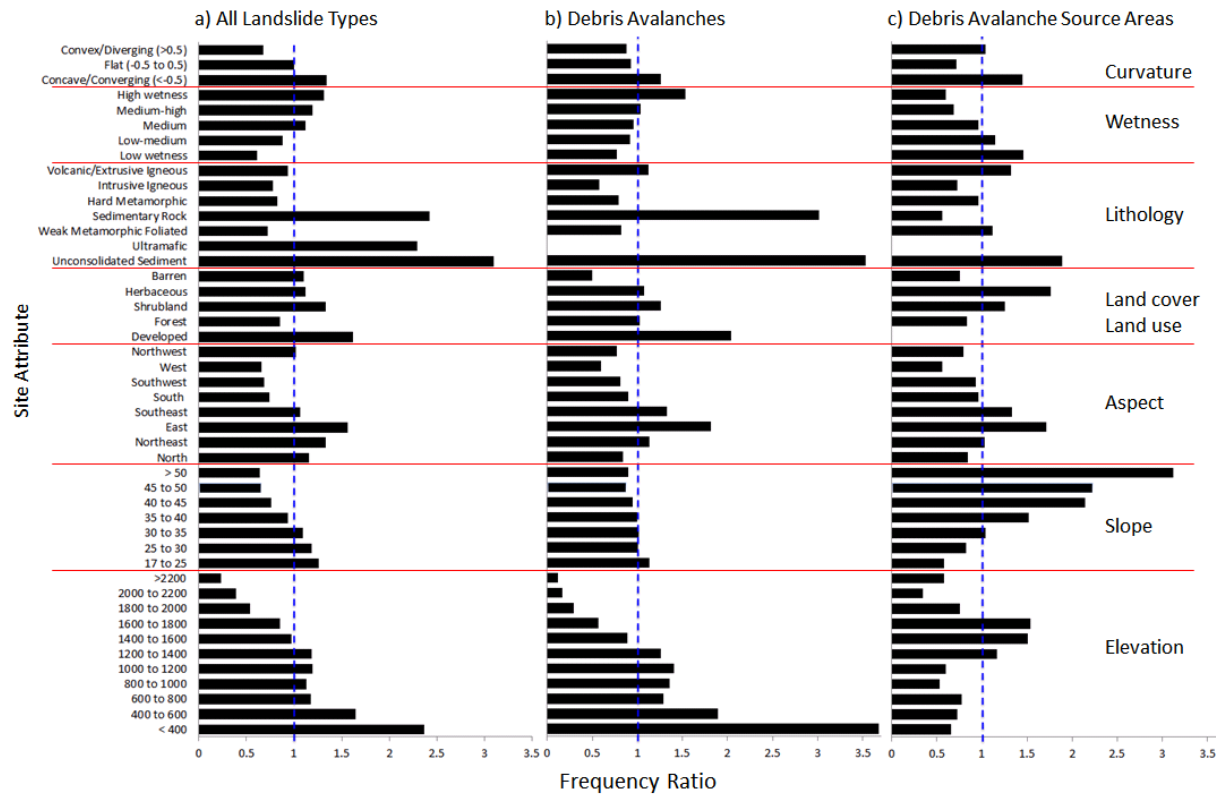
Class	WADNR Lithology	Class	WADNR Lithology	
Unconsolidated Sediments (12%)		Sedimentary Rock (2%)		
1	alluvial fan deposits	4	sedimentary deposits or rocks, undivided	
	alluvium		continental sedimentary deposits or rocks	
	alluvium, older (e.g., alluvial fans & talus)		marine metasedimentary rocks	
	alpine glacial drift, Fraser-age		marine sedimentary rocks	
	alpine glacial till, Fraser-age	Hard Metamorphic (41%)		
	glacial outwash, alpine, Fraser-age	5	banded gneiss	
	continental glacial drift, Fraser-age		mixed metamorphic and igneous rocks	
	mass-wasting deposits		orthogneiss	
2	mass-wasting deposits, mostly landslides		paragneiss	
	mass-wasting deposits, not landslides	Intrusive Igneous (21%)		
	peat deposits	6	acidic (felsic) intrusive rock	
	talus deposits		basic (mafic) intrusive rocks	
Ultramafic (0.02%)			diorite	
ultrabasic (ultramafic) rocks (<i>serpentine</i>)	gabbro			
Weak Metamorphic Foliated (14%)			granite	
heterogeneous metamorphic rocks	granodiorite			
3	hetero. metamorphic rocks, chert bearing		Intermediate intrusive rocks	
	marble		Intrusive breccia	
	metasedimentary and metavolcanic rocks		quartz diorite	
	metasedimentary rocks		quartz monzonite	
	metasedimentary rocks, cherty		tonalite	
	metavolcanic rocks	Volcanic/Extrusive Igneous (2%)		
	amphibolite	7	tuffs and tuff breccias	
	phyllite, low grade		dacite flows	
	schist, low grade		rhyolite flows	
--	Water and Ice (7%)		volcanic breccia	

3 Results and Discussion

3.1 Frequency Ratio Analysis

The results of the FR analyses for each site attribute (SA) are presented in Fig. 4. We discuss the role of SA starting with debris avalanche source areas as they are hypothesized to represent the initiation processes of shallow landslides that transform into debris avalanches. The SAs that

1 impact shallow landslide initiation could arguably play common controls on the initiation of
 2 other types of slope failures. The frequency analysis shows a clear and growing control of local
 3 slopes greater than 35° on landslide initiation, which can be considered as the internal friction
 4 angle of cohesionless sand (Fig. 4c).



6
 7 **Figure 4.** FR value for different bins of seven Site Attributes (SA) separated by red lines, based on (a) all
 8 landslide types mapped within the NOCA study domain, (b) debris avalanche landslide types only, and
 9 (c) source areas of debris avalanches represented by the highest 20% of the mapped debris avalanche.
 10 The vertical blue line refers to the FR value of 1.0, denoting when no association is found with mapped
 11 landslides. FR values below this line are attributes less likely associated with landslides and FR values
 12 above this line indicate greater association with landslides.

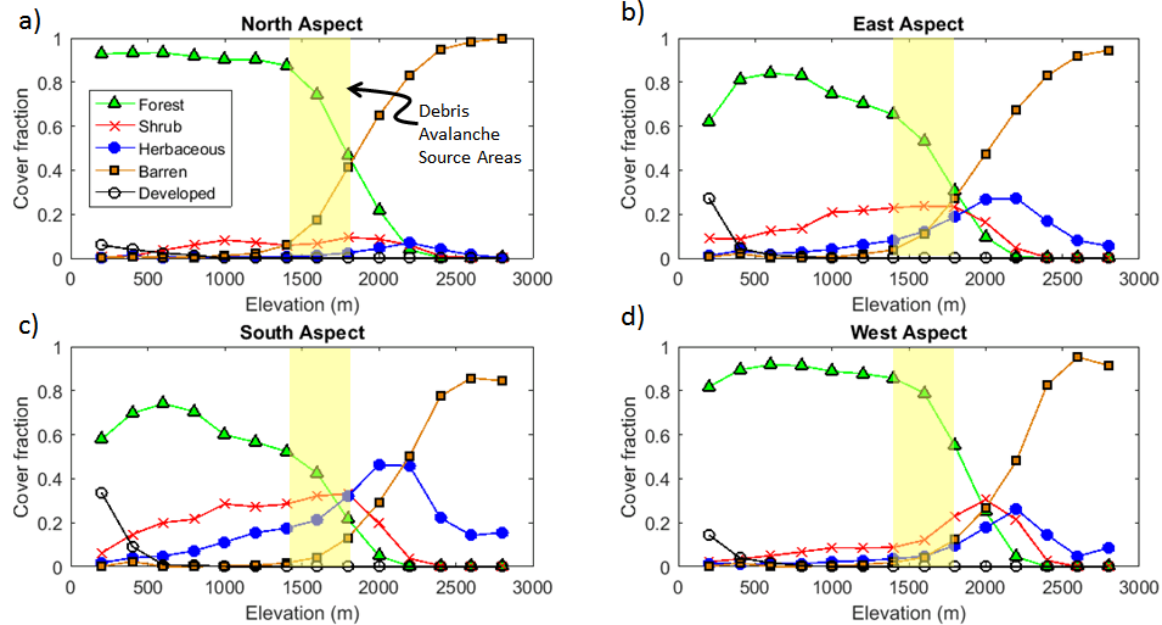
13
 14 The source area of debris avalanches is only about 17% of the mapped debris avalanche area and
 15 10% of the whole landslide inventory, which predominantly maps transport and depositional
 16 areas. A small debris avalanche source area in steep terrain can lead to large landslide impacts in
 17 lower elevations, as the eroded material travels downhill and deposits in gentler gradients (Fig.
 18 1). Thus, the runout zones of debris avalanches and other mapped landslide types cover more
 19 area at gentler slopes typical of lower elevations. This process is captured in Fig. 4a and 4b
 20 where the FR analyses exhibit higher landslide hazard at gentler slopes (<30°), more likely
 21 associated with transport and depositional processes as well as failure of side slopes along
 22 glacially incised U-shaped valleys undercut by fluvial activity. Others have reported clustering of
 23 landslide impacts in lower elevations within valleys where hillslopes are steep enough to fail
 24 (Megahan et al., 1978; Kelsey, 1988; Densmore et al., 1997; Chalkias et al., 2014).
 25

1 In the study area, local slopes generally increase on average with elevation, particularly above
2 1,400 m (Strauch et al., 2018). The control of steeper slopes on debris avalanche initiation is
3 supported by the results for elevation where source areas are associated with mid to high
4 elevation (1,400 to 1,800 m) and entire debris avalanches and all landslides types, including
5 deposition zones, have growing frequency in lower elevations (< 1,200 m) with the highest
6 frequency falling in elevations <400 m (Fig. 4a, b). Further increase in slopes typically lead to
7 bedrock exposure and barren lands with thin soil (Strauch et al., 2018; Gabet, 2003). In addition
8 to steepening slopes, the observed higher frequency of debris avalanche source areas in the mid-
9 to-high elevation range corroborates recent findings of an ecosystem transition control on
10 landslide initiation (Strauch et al., 2018). With the cooling of air temperatures beyond forest
11 ecosystem thresholds, the transition of forest vegetation (predominant alpine conifers) to mixed
12 shrub and herbaceous vegetation types with lower root cohesion, lead to higher landslide
13 frequency at debris avalanche source areas (Fig 4c). The slope and elevation results, however,
14 are likely influenced by the mapping approach, which was biased in mapping landslide activity
15 on the lower portions of hillslopes that were typically more accessible, and continuous creep and
16 rapid slides in subalpine and alpine areas were infrequently mapped.

17
18 Developed areas that include impervious surfaces, constructed materials, and lawns have the
19 highest landcover association with all mapped landslide areas, as well as with debris avalanches,
20 yet no association with debris avalanche source areas, which are typically higher on mountains
21 and rarely developed. Although dirt roads have been found to disrupt drainage and increase
22 erosion (Croke and Hairsine, 2006; Montgomery, 1994; Swanson and Dyrness, 1975), the lack of
23 association with landslide initiation suggest that these areas may be positioned on the landscape
24 in areas likely to be impacted by landslide runout or deposition~~these impacts are not evident in~~
25 ~~NOCA based on the scarcity of roads~~. In general, forest and barren landcover show the least
26 landslide activity compared to other landcover (Fig. 4). The forest association likely indicates the
27 positive contribution of root cohesion to hillslope stability, whereas the barren landcover type
28 results may indicate the effect of mapping completeness or hillslope processes. The barren
29 results appear counter to the findings of the process-based physically-based landslide model
30 applied at the same location, which found high probability of landslide initiation in barren areas
31 often below retreating glaciers (Strauch et al., 2018). Barren includes areas of bedrock, glacial
32 debris, and other accumulations of earthen material with vegetation generally accounting for less
33 than 15% of total cover; thus, there may be a variety of stability conditions within this single
34 cover class.

35
36 The sources of debris avalanches are linked to eastern and southeastern aspects (Fig. 4c); 20%
37 and 15% of source cells by area occur on these aspects, respectively. Except for western aspects
38 that show the weakest association debris avalanches, other aspects show landsliding frequency
39 close to the average frequency in the whole study domain. Vegetation type and cover that relate
40 to root strength and moisture regime can be related to aspect. East and south exposures have
41 lower forest cover fractions compared to other aspects at mid to lower elevations (< 1,400 m),
42 and forests are largely replaced by barren lands and shrub and herbaceous vegetation as elevation
43 increases (Fig. 5). Most source areas of debris avalanches and debris avalanches as a whole are
44 associated with shrub and herbaceous vegetation types (Fig. 4b,c). Other aspects, especially
45 west-facing slopes have higher fraction of forest cover (Fig. 5), likely linked to a longer growing

1 season (Evans and Fonda 1990). Lower landslide frequency in western aspects can be a result of
 2 higher root cohesion of forest vegetation compared to shrub and herbs. Additionally, perhaps
 3 west-facing aspects experience more arid moisture regimes or bedrock bedding, jointing, or
 4 fracturing conducive to stability compared to other exposures (Carson and Kirby, 1972; Fischer
 5 et al., 2006).



6
 7 **Figure 5.** Vegetation cover fraction in NOCA on each aspect, taken as the fraction of vegetation type
 8 within each 200-m elevation band. Aspects categorized here as **a)** north (0° to 45° and 315° to 360°), **b)**
 9 east (45° to 135°), **c)** south (135° to 225°), and **d)** west (225° to 315°), covering 23%, 23%, 26%, and
 10 28% of NOCA, respectively. Yellow highlighted area represents the strongest elevation association for
 11 debris avalanche source areas.

12 When all landslides are considered, northern slopes exhibit growing landslide association while
 13 landslide frequency declines in southeastern slopes [compared to the other landslide datasets](#) (Fig.
 14 4a, b). North-facing slopes have been documented to retain more soil moisture than south-facing
 15 aspects in northern latitudes (Geroy et al., 2011), which can be broadly responsible for more
 16 initiation, transport and deposition impact of all mass wasting types. Hillslope asymmetry (i.e.,
 17 steeper slopes depending on aspect) was not found during inspection of average slope on the four
 18 primary aspects. North-south asymmetry has been found to demonstrate reversal based on
 19 elevation and at 49° latitude, which correspond to the northern edge of NOCA (Poulos et al.,
 20 2012). In general, the relatively similar aspect associations for different landslide observation
 21 datasets likely indicates the connection of source areas to downstream processes of transport and
 22 deposition (Fig. 1).

23 Comparisons among all landslides, whole debris avalanches, and debris avalanche source areas
 24 clearly show that unconsolidated sediments, largely derived from transport and depositional
 25 processes, have stronger association with landslides than other lithologies followed by
 26 sedimentary rock (Fig. 4). This strong association is expected given the inclusion of mass
 27 wasting landforms in the classification of unconsolidated sediment. The high ultramafic rock
 28 association when considering all landslide types is driven by a single topple/fall occurring in this

1 scarce lithology (<0.02% of NOCA). Widespread observation of debris avalanche source areas in
2 all rock types may point to the role of steep slopes regardless of lithology. For debris avalanche
3 processes, sedimentary rock is more associated with transport and depositional areas than source
4 areas. Areas without landslide activity were associated with weak metamorphic foliated and
5 intrusive igneous lithology (Fig. 4a).

6
7 The association of landslides on concave/converging versus convex/diverging topography is
8 relatively consistent among the datasets and generally consistent with literature due to enhanced
9 wetness where vegetative support may be weak in deeper soils (see Hales et al., 2009; Fig. 4).
10 High wetness index is associated with landslides for all landslide types as well as entire debris
11 avalanches (Fig. 4a,b). This result is intuitive as this index is an indicator of increased soil
12 saturation and surface runoff. In contrast, source areas were correlated with low wetness index
13 (Fig. 4c). This counterintuitive finding, however, aligns with previously discussed results that
14 source areas are associated with loss of root strength, steep slopes and higher elevations,
15 resulting in relatively small specific catchment areas. By definition, wetness index is negatively
16 correlated with slope and positively correlated with specific contributing area. Thus, source
17 areas will have a low wetness index when they are from steep slopes with small contributing
18 areas (i.e., located higher up on hillslopes).

19
20

3.2 Susceptibility Index

21 A susceptibility index (SI) is calculated for each grid cell within the study area domain by
22 equation (3). Cumulative distributions for SI, plotted as fraction of area of the study domain as
23 well as only in the areas where landslide impact was mapped show higher SI values for a given
24 fraction of the respective domains where a given SI is exceeded (Fig. 6a, d, and g). Additional
25 support beyond the graphics that these distributions are not equal is provided by the
26 Kolmogorov-Smirnov test, which rejects the null hypothesis of equal distributions at $\alpha < 0.01$. The
27 cumulative distributions show that the SI calculated from FR method can differentiate mapped
28 landslide locations from non-landslides with a larger SI. The resulting spatial distribution of SI is
29 right skewed as shown in the relative frequencies of SI for all three landslide datasets (Fig. 6b, e,
30 and h). The right skew indicates that there is a small population of grid cells with high SI
31 compared to the majority of grid cells in the study domain. This occurs when there are FR
32 subcategories frequently associated with landslides coinciding at the same location. Histograms
33 show a greater relative frequency of landslide grid cells with high SI values than the entire
34 domain (Fig. 6b, e, and h). For source areas, SI bins for the histograms were larger (e.g., 0.5 vs
35 0.25) due to the small number of source area cells compared to the two other datasets.
36

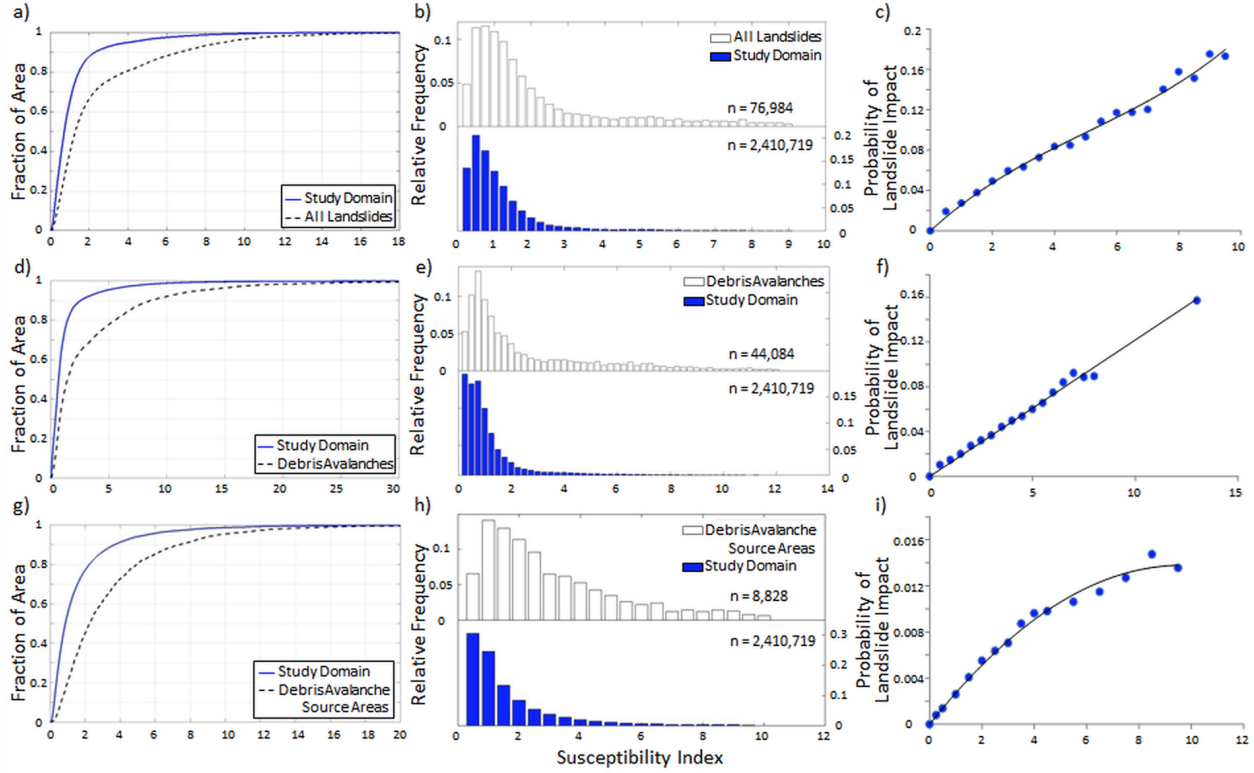


Figure 6. Cumulative distributions (**a**, **d**, and **g** - column 1) and relative frequency plots (**b**, **e**, and **h** - column 2) of Susceptibility Index (SI) for all grid cells included in the analysis and the grid cells contained within mapped landslides. *Third column (c, f, and i)* is the probability of landslide impact, $P(LS_r|SI_r)$, calculated from the ratio of the number of landslide cells to the number of all cells with each SI bins with fitted curves. *Rows represent analysis domains: a, b, and c) all landslide types; d, e, and f) debris avalanches; and g, h, and i) debris avalanche source areas.*

The probability of landslide impact, $P(LS_r|SI_r)$, calculated from Eq. (4) are shown in the third column of Figure 6 (Fig. 6c, f, and i). In calculating this probability in the highest SI bins (e.g., $SI \geq 8$), landslide sample sizes of about 500 or fewer were aggregated into the previous bin. In all three cases, $P(LS_r|SI_r)$ increases with SI, supporting the statistical power of this empirical approach. The SI to $P(LS_r|SI_r)$ relation is explained by a linear function when debris avalanche data are used (Fig. 6f). The other two cases, all landslide data and debris avalanche source areas, are better represented by polynomial fits (Fig. 6c and i). The range of probabilities grows with the sample size of the landslide dataset used, leading to maximum probabilities of 0.2, 0.16, and 0.017 for all landslide, debris avalanches, and debris avalanche source areas, respectively. These functions were used to develop continuous empirical probability maps based on SI values assigned to each grid cell of the study domain, -limited to the maximum empirical probability of each landslide type.

3.3 Landslide Hazard Maps

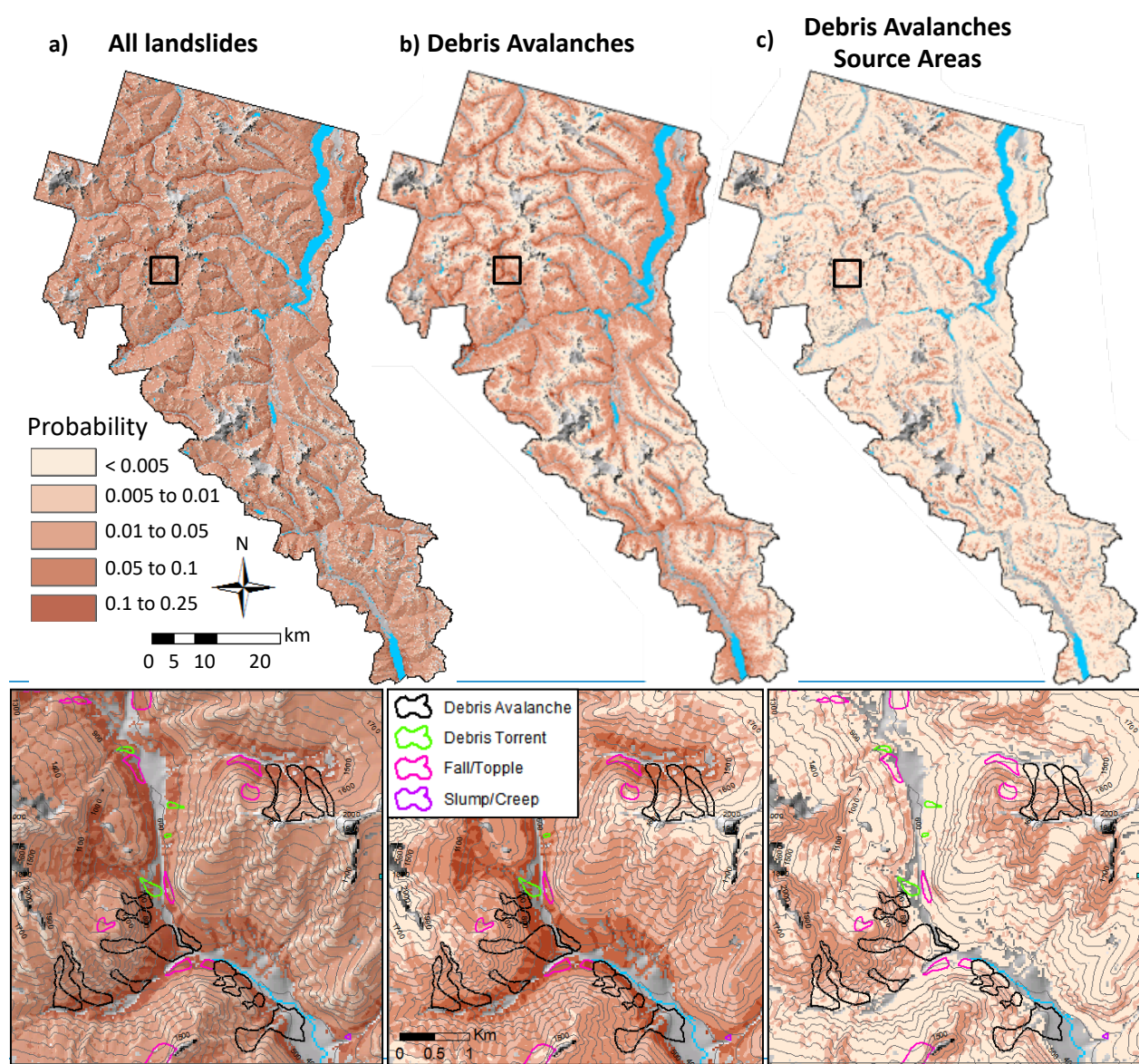
The probability of landslide impact estimated from SI, $P(LS_r|SI_r)$, declines as the amount of observational information decreases from all landslides (Fig. 7a), to debris avalanches (Fig. 7b), and debris avalanche source areas (Fig. 7c). This pattern reflects the smaller area of observed landslide data used in each case compared to the study domain. Additionally, the probability of

any landslide activity would be expected to be higher than the probability of initiating a debris avalanche alone. When considering all landslides, the highest probabilities are located near the base of valley walls and in topographic depressions or hollows (Fig. 7a). The hazard map developed from the empirical model using only debris avalanches (Fig 7b) also shows higher probabilities in the valley bottoms, but lower probabilities than the all landslides map at higher elevations in alpine areas where the footprint of debris avalanches is smaller compared to the deposition area, reducing the overall probabilities in the FR approach. Spatial patterns of landslide probabilities obtained from the source areas of debris avalanches (Fig. 7c) departs from the other two empirical models with the highest probabilities in middle and upper portions of valley walls, similar to the process model (Fig. 8b). Thus, the empirically-based modeling using only source areas appears to capture some of the physical processes initiating debris avalanches. Closeup areas mapped for each mapping case more clearly illustrate the landslide hazard in relation to topographic position.

We developed a map of annual probability of shallow landslide initiation by combining the empirical SI-based probability (Fig 7c) and the [process-basedphysically-based](#) annual probability of landslide initiation from Strauch et al. (2018), $P(FS_c \leq 1)$, using the methodology developed in this paper (Eq. 8 and 9). The weight term, $P(FS_c \leq 1)$, and the P(LS) are shown in Fig. 8. Close ups of three locations are shown below the full NOCA maps.

Approximately 30% of the analyzed cells had weights > 1 . Weights are greater in high elevations and steep slopes, commensurate with debris avalanche source areas. Overall 88% of the NOCA area has less than annual landsliding probability of 0.1 in $P(FS_c \leq 1)$ and P(LS) map. P(LS) map (Fig. 8c and f) shows enhanced landslide probability in areas already modeled as high probability of landslide impacts based on the [processed-basedphysically-based](#) shallow landslide model (Fig. 8b and e). An anomaly map created by subtracting P(LS) from $P(FS_c \leq 1)$ provides easier display of the effect of the empirical adjustment. In the anomaly map, much of the original $P(FS_c \leq 1)$ is adjusted by less than ± 0.1 (Fig. 9). East-facing aspect, concave curvature, and elevations in the $\sim 1,000$ to $1,600$ m range show an increase in probability > 0.1 (Fig. 9). Increasing probabilities on east-facing slopes compared to other aspects aligns with the FR findings (Fig. 4).

32



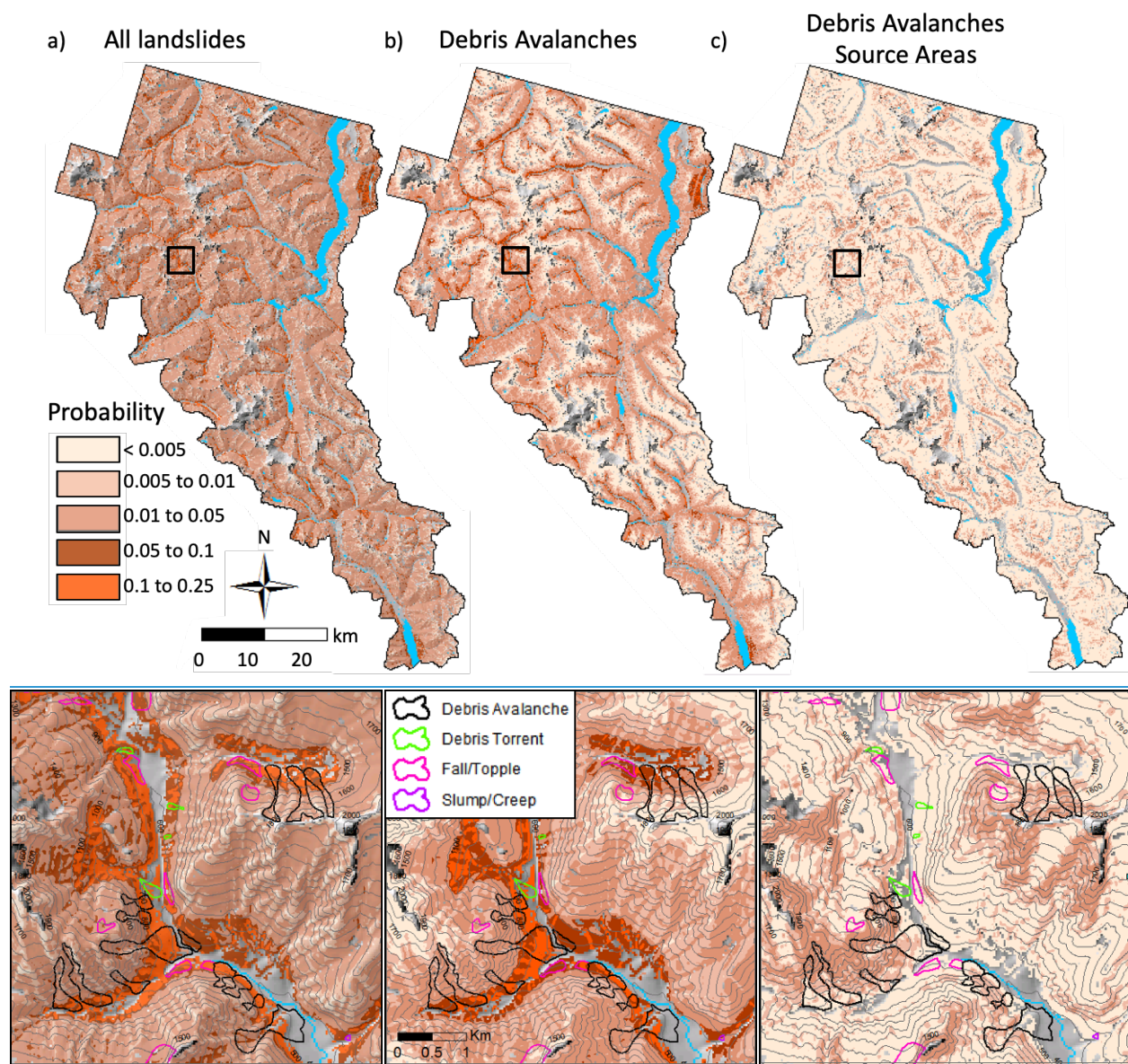
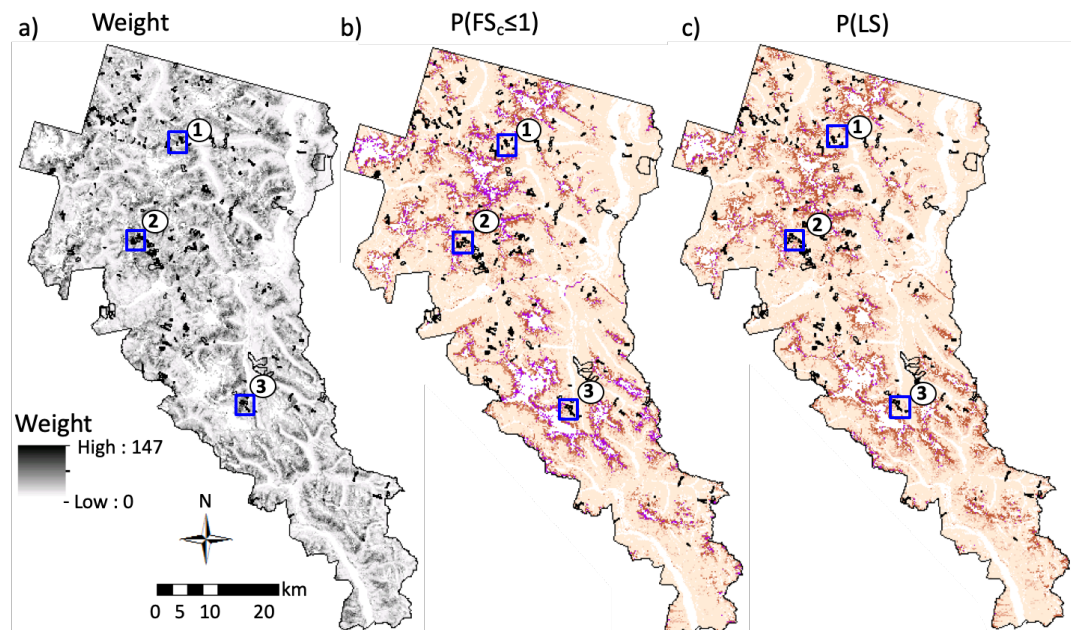
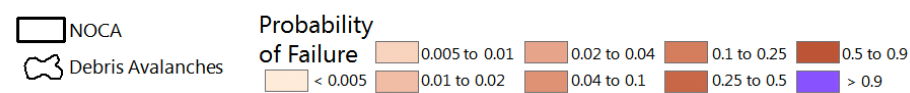
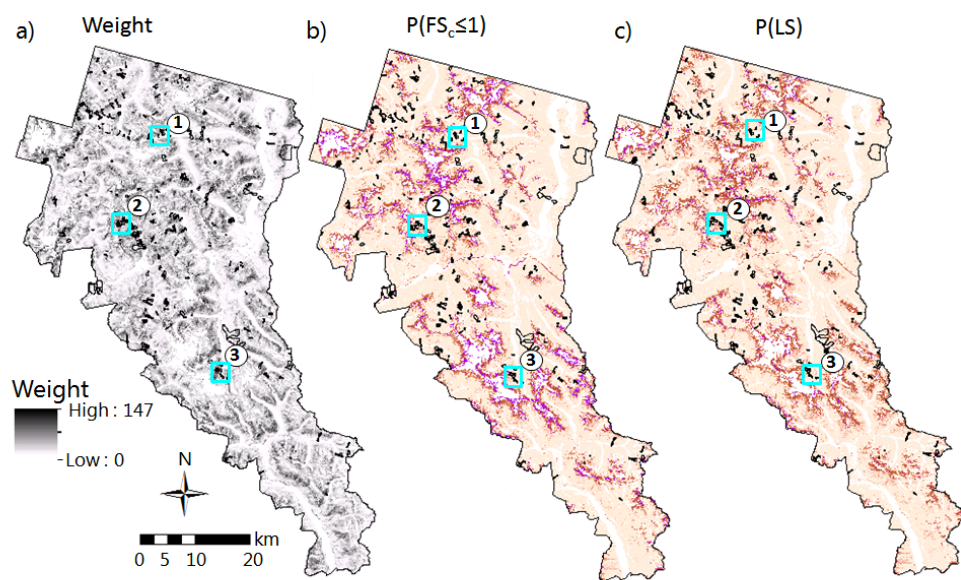


Figure 7. Maps of probability of landslide impact derived from empirical model based on: **a)** all landslide types, **b)** debris avalanches, and **c)** and source areas of debris avalanches overlain on hillshade raster. Black boxes indicate closeup areas shown below with overlain landslide types and 100 m contours. Gray areas excluded from analysis show river valleys and glaciated crests.



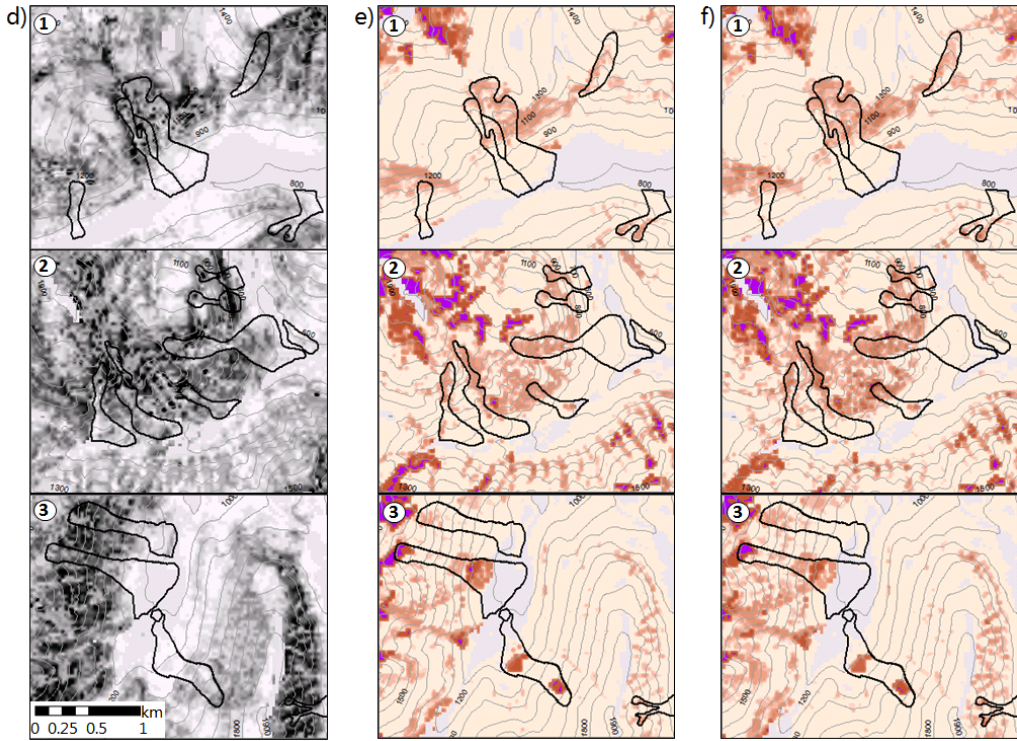


Figure 8. Maps of: **a)** weight term derived from joint empirical and [physically-based](#) modeled probabilities, **b)** $P(FS_c \leq 1)$ from Strauch et al. (2018), and **c)** $P(LS)$ created from multiplying a) by b) at each grid cell for the North Cascades National Park Complex (NOCA). Blue boxes indicate three closeup locations shown below in **d), e),** and **f)**. Black lines show mapped debris flow boundaries. Gray areas are excluded from analysis and contours are at 100 m.

Other cells declined in probability, particularly on gentler slopes, north to west-facing aspects, and at low (< 1000 m) and high ($> 1,600$ m) elevations (Fig. 9). Areas with reduced probability high on the mountain, above the elevation limit of vegetation ($\sim 2,200$ m, Fig. 5) and just below actively receding glaciers or permanent snowfields, likely represent limited soil development and active surface erosion where slopes are steep (Roering et al., 2003) (Fig. 9). Within the elevation range of the park, debris avalanche initiation is not frequently observed at the highest elevations where soil is thin or the landscape is covered seasonally by snow and ice.

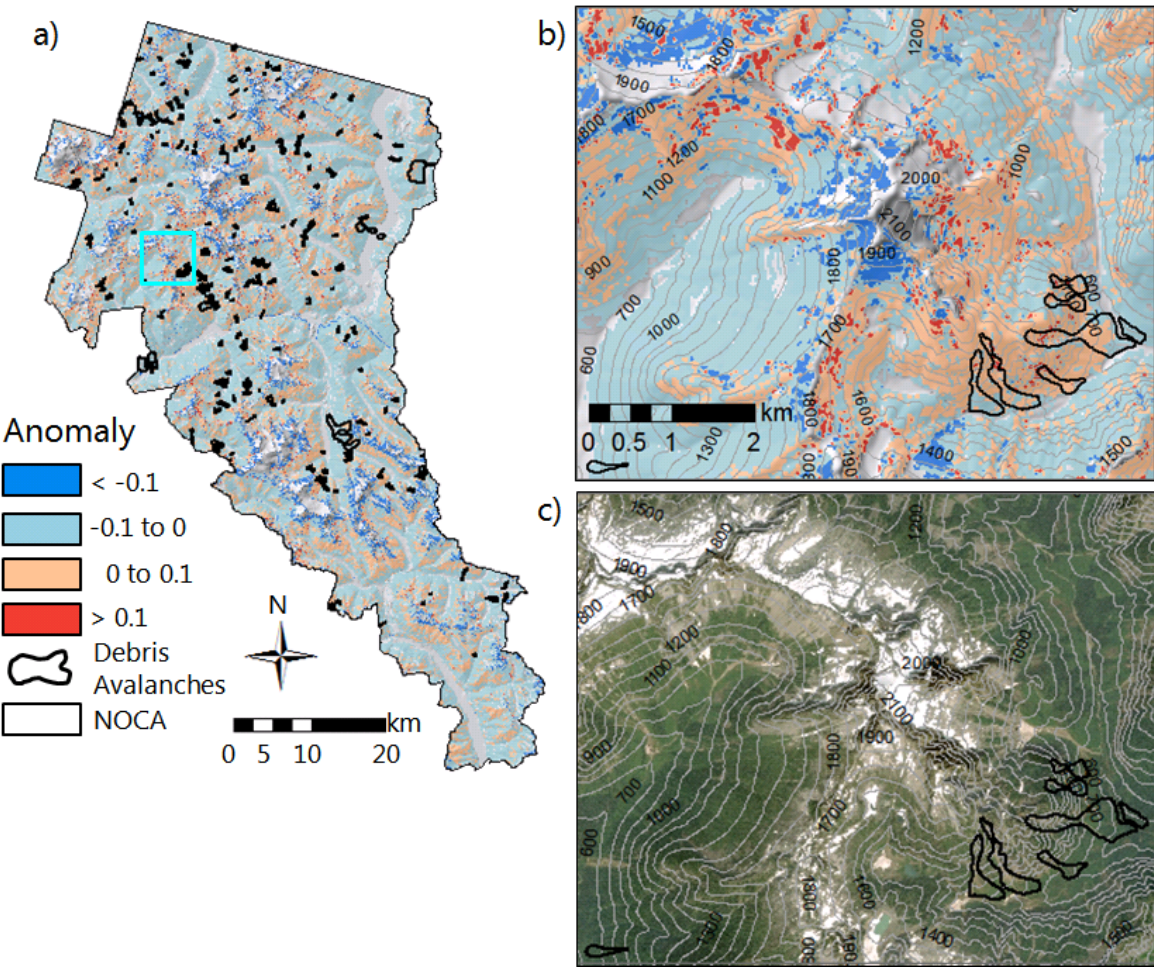
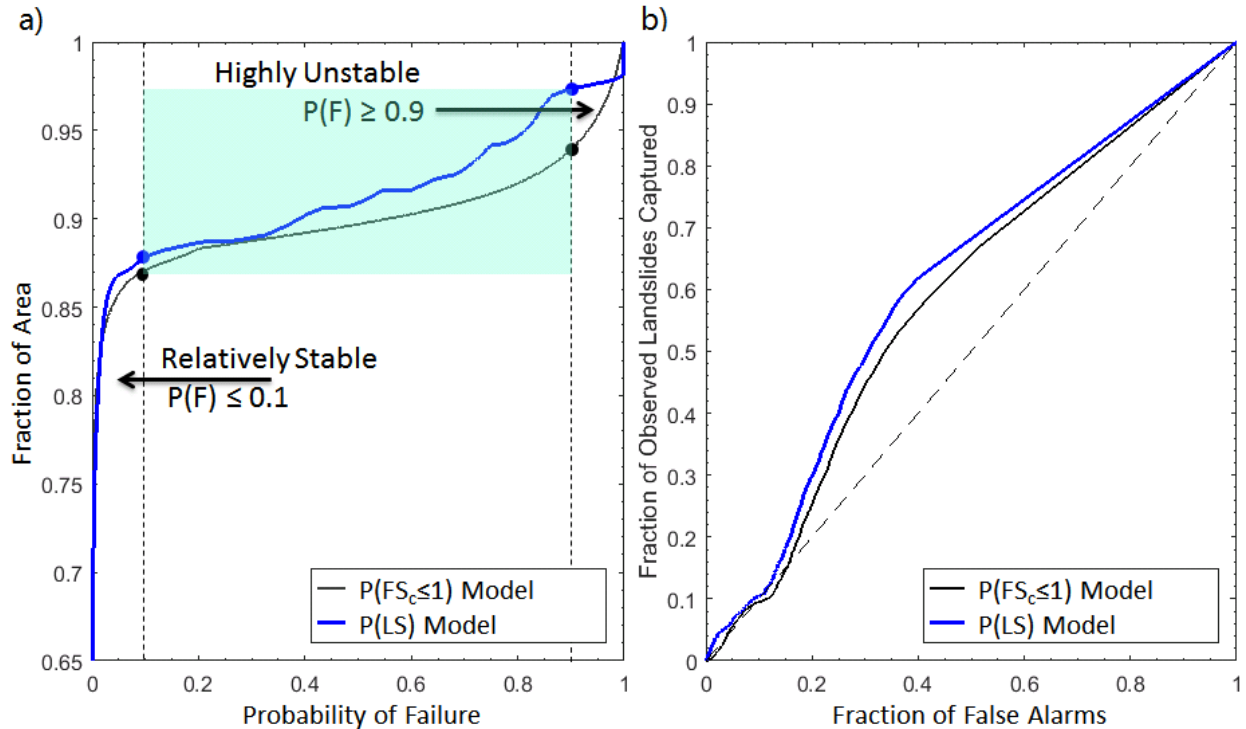


Figure 9. Anomaly maps displaying the difference between $P(LS)$ and $P(FS_c \leq 1)$ where blues represent > 0.1 reduction in probability and reds represent > 0.1 increase in probability due to the empirical adjustment. Maps of: **a)** the entire North Cascades National Park Complex, **b)** closeup location indicated by blue-cyan box in a) overlain on hillshade raster, and **c)** aerial image of the same location as b). Aerial image is from World Imagery, Esri Inc. (images created using ArcGIS® software by Esri. ArcGIS® and ArcMap™ are the intellectual property of Esri and are used herein under license. Copyright Esri©. All rights reserved. For more information about Esri® software, please visit www.esri.com). Gray areas are excluded from analysis and contours are at 100 m.

To investigate the spatial distribution of $P(FS_c \leq 1)$ (Strauch et al., 2018) and empirically-adjusted model probabilities, $P(LS)$, we plot the cumulative distributions of probabilities (Fig. 10a). In ~~approximately~~^{roughly} 12⁵% of the NOCA domain, $P(LS)$ gives lower landslide probability than $P(FS_c \leq 1)$, indicated by the upward shift in the cumulative distribution (blue line) (Fig. 10a). ~~This suggest an overall reduction in landslide probability at the broad landscape scale when empirical data is used in weighting factors, except where $P(FS_c \leq 1)$ is already near 1.0.~~ The modeled landscapes have $P(\text{Failure}) \geq 0.9$, ~~or recurrence interval ≤ 1.1 year~~, in ~6% and ~3% for $P(FS_c \leq 1)$ and $P(LS)$ models, respectively (Fig. 10a). These cells represent highly unstable slopes and the empirical adjustment reduced this area by half from the ~~processed-based~~^{physically-based} model. Unconditionally unstable landslide, $P(\text{Failure})=1$ (Pack et al., 1998; Montgomery, 2001), corresponds to 0% and 2% of $P(FS_c \leq 1)$ and $P(LS)$ models,

respectively. Unconditionally stable slopes, $P(\text{Failure})=0$, corresponds to 49% of the study domain for both $P(FS_c \leq 1)$ and $P(\text{LS})$ models (not visible in Fig. 10a). The distributions generally show a high portion (~87 to 88%) of the modeled landscapes has relatively low $P(\text{Failure}) \leq 0.1$, probability of failure, $P(FS_c \leq 1)$ or a return period of ≥ 10 years. Thus, the empirical information provides most of the hazard adjustments to the areas in between unconditionally stable and unconditional unstable conditions. Only between 7% and 9% of the landscape has a broad-wide range of potential failure ($0.1 \leq P(\text{Failure}) \leq 0.9$) as indicated by the shaded blue (Fig. 10a), where empirical evidence enhanced the local landscape susceptibility to initiation of shallow landslides.



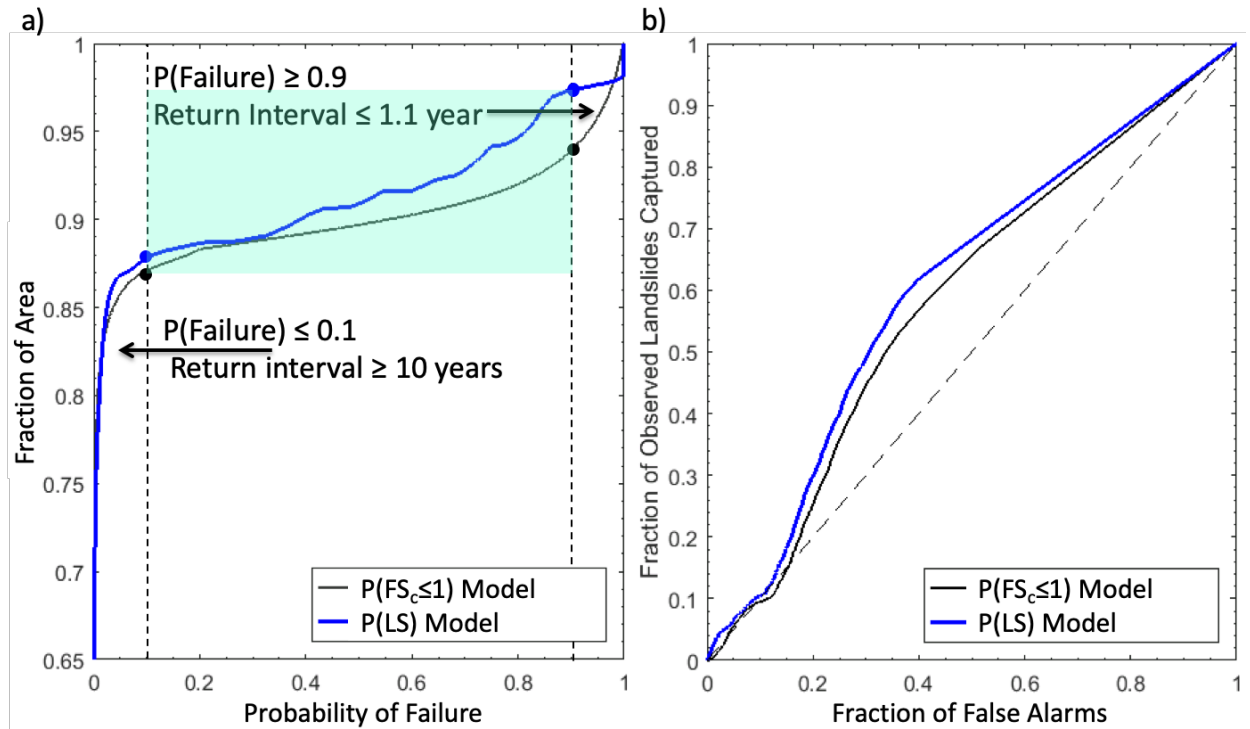


Figure 10. a) Cumulative distribution of the probability of failure for the $P(FS_c \leq 1)$ [black] and $P(LS)$ [blue] using only debris avalanche source areas, b) ROC curves for the same two datasets. The blue shaded area on a) represents the fraction of the landscape with $0.1 \leq P(\text{Failure}) \leq 0.9$. Black diagonal dashed line on a 1 : 1 line in b) represents the case of a trivial or random classification model. AUC values are 0.58 for the modeled probability and 0.60 for the integrated probability.

We anticipated that the additional consideration of the empirical model represented by the weighting term improves the performance of the purely processed-basedphysically-based model. Thus, to assess the potential performance of the models, we statistically evaluated the models using the receiver operating characteristics (ROC) curves (Fawcett, 2006). This approach examines cells within mapped landslides and cells outside landslides for a study area and compares this to randomly distributed landslides over the same landscape. Confusion matrices are generated from observed and modeled landslides based on varying the probability of a landslide threshold used to generate ROC curves (Mancini, et al., 2010; El-Ramly et al., 2002; Anagnostopoulos et al., 2015) (Fig. 10b). A better-performing model curves towards the upper left corner, and a curve along the 1:1 line represents a trivial model that randomly assigns landslide and non-landslide cells. The area under the curve (AUC) statistic provides a numerical indicator of model performance representing the probability of correctly assigning two randomly selected cells to landslide and non-landslide datasets (Hanley and McNeil, 1982).

Both the processed-basedphysically-based model, $P(FS_c \leq 1)$, and the $P(LS)$ perform better than a trivial model by plotting the ROC curve above the 1:1 line (Fig. 10b). The AUC statistic was 0.58 and 0.60 for $P(FS_c \leq 1)$ and $P(LS)$, respectively. The ROC and AUC indicate an improvement in the fraction of observed landslides captured by $P(LS)$ over $P(FS_c \leq 1)$. The AUC for $P(LS)$ indicates that there is a 60% chance that the proposed empirical adjustment to the

~~process-based physically-based~~ model would classify a landslide initiation cell and a non-landslide cell correctly from two randomly sampled grid cells. The ROC analysis found that the optimum probability threshold for maximizing the observed landslides captured and minimizing false alarms was a probability threshold of 0.0006 (i.e., apex of the blue curve); thresholds less than this increased the false alarms and thresholds greater than this reduced the accuracy of capturing observed landslides (Fig. 10b). The additional information from empirical modeling modestly improved the ~~processed-based physically-based~~ model and indicates empirical evidence on landslides can capture mechanisms lacking in the infinite slope stability model. These include clustering of debris avalanches due to variability in the bedrock geology (e.g. hydrothermal alteration, steeply dipping bedding planes, and glacial oversteepening). Additional validation approaches, such as separating landslide data into training and testing datasets, may yield additional findings that are deferred to future studies.

4 Conclusions

Empirically-based probability hazard maps were developed from a statistically-based susceptibility index, which integrated the influence of site attributes on observed landslides based on a frequency ratio approach. Resulting susceptibility depends on the observations of landslides considered: all types of landslides, debris avalanches only, or source areas of debris avalanches. Thus, the objectives of a hazard identification study dictate the necessary inventory of landslide features. The empirically-based probability model based on source areas was used to adjust a previously developed ~~processed-based physically-based~~ probabilistic model through a calculated weighting term developed from a joint spatial probability. The frequency analysis, hazard map development, and integrated probability model identified several key findings when applied to a national park:

- Frequency analysis shows a clear and growing control of local slopes greater than 35° on landslide initiation, while higher landslide hazard at gentler slopes (<30°) reflects transport and depositional processes.
- Debris avalanche source areas are associated with mid to high elevation (1,400 to 1,800 m), while all landslides types and whole debris avalanches have growing impact in lower elevations (< 1,200 m) with the highest impact falling in elevations <400 m.
- Slope is a key attribute for the initiation of landslides, while lithology is mainly tied to transport and depositional processes.
- The transition from subalpine to alpine herbaceous vegetation with lower root cohesion correlates with higher frequency of debris avalanche initiation.
- East (west) aspect is a positive (negative) landslide-influencing factor, likely due to differences in moisture regime, and forest cover and associated root cohesion.
- Empirical statistical modeling used to adjust a ~~process-based physically-based~~ model of landslide initiation improved predictability of observed landslides by accounting for additional factors that influence the landscape susceptibility to failure not represented in the physically-based model.
- Empirical adjustments generally lowered the probability of failure of the ~~process-based physically-based~~ model, especially for $0.1 \geq P(\text{failure}) \leq 0.9$ that covered between 7 to 9% of the study area park.

As the occurrence of landslide runout is conditioned on the failure of source areas, future studies could combine the probabilistic initiation methodology we propose in this paper with a landslide runout model to improve prediction of hazards from entire landslides. The applicability of our approach to characterize shallow landslides hazard is limited by the quality of the site-specific data on soils and vegetation, extent of hydrologic modeling, as well as the accuracy and completeness of the landslide inventory. Accurate data for environmental variables such as geology, soils, and vegetation would be as important as comprehensive landslide data as the empirical approach relates landslide hazard to the environmental variables. Although the approach is applicable elsewhere, our results from the empirical analyses are specific to the region in which they were developed and may differ in another location with different geology and landslide inventories. Additionally, the probabilities are likely to change as local conditions change from disturbance such as fire or as climate continues to change. Advancements in surface terrain delineation and in distributed hydrologic modeling specifically contribute to the broad applicability of this approach. We provide multiple landslide hazard maps for the national park that land managers can use for planning and decision making, as well as educating the public about hazards from landslides so they can minimize risks from these geohazards.

Author contributions. RS and EI designed the research, developed the models, performed the simulations, and created figures. JR provided landslide and geology data as well as insights on the approach and model demonstrationinsights. RS prepared the manuscript with contributions from all co-authors.

Competing interest. The authors declare that they have no conflict of interest.

Acknowledgements. This research was supported by the US National Science Foundation (CBET-1336725, ICER: 1663859, PREEVENTS) and USGS Northwest Climate Adaptation Science Center. We thank Stephen Dorsch of North Cascades National Park Complex for providing electronic copies of landslide data and reports. Dan Miller and Christina Bandaragoda provided helpful suggestions on preliminary results.

References

Agee, J. K., and Kertis, J.: Forest types of the north Cascades National Park Service complex. *Can. J. Botany*, 65(7), 1520-1530, 1987.

Aleotti, P. and Chowdhury, R.: Landslide hazard assessment: summary review and new perspectives. *Bulletin of Engineering Geology and the environment*, 58(1), 21-44 pp., 1999.

Anagnostopoulos, G. G., Fatichi, S., and Burlando, P.: An advanced process-based distributed model for the investigation of rainfall-induced landslides: The effect of process representation and boundary conditions. *Water Resour. Res.*, 51(9), 7501-7523, 2015.

Ayalew, L., Yamagishi, H., and Ugawa, N.: Landslide susceptibility mapping using GIS-based weighted linear combination, the case in Tsugawa area of Agano River, Niigata Prefecture, Japan. *Landslides*, 1(1): 73-81, 2004.

Baum, R.L., Galloway, D.L., and Harp, E.L.: Landslide and land subsidence hazards to pipelines: U.S. Geological Survey Open-File Report 2008-1164, 192 pp., 2008.

Beatty, C.B.: Landslides and Slope Exposure. *J. Geol.*, 64:1, 1956.

Bellugi, D., Milledge, D.G., Dietrich, W.E., Perron, J.T., and McKean, J.: Predicting shallow landslide size and location across a natural landscape: Application of a spectral clustering search algorithm. *J. Geophys. Res.-Earth*, 120(12): 2552-2585, 2015.

Beven, K. J., and Kirkby, M. J.: A physically based, variable contributing area model of basin hydrology. *Hydrolog. Sci. J.*, 24(1): 43-69, 1979.

Bordoni, M., Meisina, C., Valentino, R., Bittelli, M., and Chersich, S.: Site-specific to local-scale shallow landslides triggering zones assessment using TRIGRS, *Nat. Hazard. Earth Sys.*, 15(5): 1025-1050, 2015.

Borga, M., Fontana, G.D., and Cazorzi, F.: Analysis of topographic and climatic control on rainfall-triggered shallow landsliding using a quasi-dynamic wetness index. *J. Hydrol.*, 268(1): 56-71, 2002.

Carrara, A., Cardinali, M., Guzzetti, F., and Reichenbach, P.: GIS technology in mapping landslide hazards, in: *Geographical Information System in Assessing Natural Hazard*, edited by: Carrara, A., and Guzzetti, F., Springer, Dordrecht, 135-175 pp., 1995.

Carson, M. A., and Kirkby, M. J.: *Hillslope Form and Process*, Cambridge Univ. Press, Cambridge, U.K., 475 pp., 1972.

Cevasco, A., Pepe, G., and Brandolini, P.: The influences of geological and land use settings on shallow landslides triggered by an intense rainfall event in a coastal terraced environment. *B. Eng. Geol. Environ.*, 73(3): 859-875, 2014.

Chalkias, C., Ferentinou, M., and Polykretis, C.: GIS-based landslide susceptibility mapping on the Peloponnese Peninsula, Greece. *Geosciences*, 4(3), 176-190, 2014.

Chung, C. F., Fabbri, A. G., and Van Western, C. J.: Multivariate regression analysis for landslide hazard zonation, in: *Geographical Information System in Assessing Natural Hazard*, edited by: Carrara, A. and Guzzetti, F., Springer, Dordrecht, 107-133, 1995.

Coe, J. A.: Landslide hazards and climate change: A perspective from the United States, in: *Slope safety preparedness for impact of climate change*, Chapter: 14., edited by: Ho, K., Lacasse, S., and Picarelli, L., CRC Press, Boca Raton, FL., 479-523 pp., 2016.

Collins, B. D., and Montgomery, D. R.: The legacy of Pleistocene glaciation and the organization of lowland alluvial process domains in the Puget Sound region. *Geomorphology*, 126(1): 174-185, 2011.

Corominas, J., Van Westen, C., Frattini, P., Cascini, L., Malet, J. P., Fotopoulou, S., Catani, F., Van Den Eeckhaut, M., Mavrouli, O., Agliardi, F., and Pitilakis, K.: Recommendations for the quantitative analysis of landslide risk. *B. Eng. Geol. Environ.*, 73(2): 209-263, 2014.

Croke, J. C., and Hairsine, P. B.: Sediment delivery in managed forests: a review. *Environ. Rev.*, 14(1), 59-87, 2006.

Crozier, M. J.: Deciphering the effect of climate change on landslide activity: A review. *Geomorphology*, 124(3): 260-267, 2010.

Dai, F.C., Lee, C.F.: Landslide characteristics and slope instability modeling using GIS, Lantau Island, Hong Kong. *Geomorphology* 42:213-228, 2002.

Densmore, A.L., Anderson, R.S., McAdoo, B.G., and Ellis, M.A.: Hillslope evolution by bedrock landslides, *Science*, 275: 369-372, 1997.

El-Ramly, H., Morgenstern, N. R., and Cruden, D. M.: Probabilistic slope stability analysis for practice, *Can. Geotech. J.*, 39, 665-683, 2002.

[Ercanoglu, M., and Sonmez, H.: General Trends and New Perspectives on Landslide Mapping and Assessment Methods. In Environmental Information Systems: Concepts, Methodologies, Tools, and Applications, pp. 64-93. IGI Global, 2019.](#)

Evans, R. D., and Fonda, R. W.: The influence of snow on subalpine meadow community pattern, North Cascades, Washington. *Can. J. Botany*, 68(1): 212-220, 1990.

Fawcett, T.: An introduction to ROC analysis, *Pattern Recogn. Lett.*, 27(8):861-874, 2006.

Fischer, L., Kääb, A., Huggel, C., and Noetzli, J.: Geology, glacier retreat and permafrost degradation as controlling factors of slope instabilities in a high-mountain rock wall: the Monte Rosa east face. *Nat. Hazard. Earth Sys.*, 6(5): 761-772, 2006.

Gabet, E. J.: Sediment transport by dry ravel. *J. Geophys. Res.-Sol. Ea.*, 108(B1), 2003.

Geroy, I. J., Gribb, M. M. Marshall, H. P. Chandler, D. G. Benner, S. G. and McNamara, J. P.: Aspect influences on soil water retention and storage. *Hydrol. Process.*, 25, 3836-3842, doi:10.1002/hyp.8281, 2011.

Ghirotti, M.: The 1963 Vajont landslide, Italy, in: *Landslides: Types, mechanisms and modeling*, edited by: Claque, J. J. and Stead, D. Cambridge University Press, NY., 359 pp, 2012.

Gokceoglu, C., Sonmez, H., Nefeslioglu, H. A., Duman, T. Y., and Can, T.: The 17 March 2005 Kuzulu landslide (Sivas, Turkey) and landslide-susceptibility map of its near vicinity. *Eng. Geol.*, 81(1): 65-83, 2005.

Gupta, R. P., and Joshi, B. C.: Landslide hazard zoning using the GIS approach—a case study from the Ramganga catchment, Himalayas. *Eng. Geol.*, 28(1): 119-131, 1990.

Haeberli, W., Schaub, Y., Huggel, C.: Increasing risks related to landslides from degrading permafrost into new lakes in de-glaciating mountain ranges. *Geomorphology*: <https://doi.org/10.1016/j.geomorph.2016.02.009>, 2016.

Hales, T. C., Ford, C. R., Hwang, T., Vose, J. M., and Band, L. E.: Topographic and ecologic controls on root reinforcement, *J. Geophys. Res.*, 114, F03013, doi:10.1029/2008JF001168, 2009.

Hamlet, A. F., Elsner, M. M., Mauger, G., Lee, S., and Tohver, I.: An Overview of the Columbia Basin Climate Change Scenarios Project: Approach, Methods, and Summary of Key Results, *Atmos. Ocean.*, 51, 392-415, 2013.

Hanley, J. A. and McNeil, B. J.: The meaning and use of the area under a receiver operating characteristic (ROC) curve, *Radiology*, 143, 29-36, 1982.

Haugerud, R.A., and Tabor, R.W.: Geologic map of the North Cascade Range, Washington, US Department of the Interior, U.S. Geological Survey, 29 pp., 2009.

Hobley, D. E. J., Adams, J. M., Nudurupati, S. S., Hutton, E. W. H., Gasparini, N. M., Istanbulluoglu, E., and Tucker, G. E.: Creative computing with Landlab: an open-source toolkit for building, coupling, and exploring two-dimensional numerical models of Earth-surface dynamics, *Earth Surf. Dynam.*, 5, 21-46, <https://doi.org/10.5194/esurf-5-21-2017>, 2017.

Hong, H., Chen, W., Xu, C., Youssef, A. M., Pradhan, B., and Tien Bui, D.: Rainfall-induced landslide susceptibility assessment at the Chongren area (China) using frequency ratio, certainty factor, and index of entropy. *Geocarto Int.*, 32(2): 139-154, 2017.

Hungr, O., Leroueil, S., and Picarelli, L.: The Varnes classification of landslide types, an update. *Landslides*, 11(2): 167-194, 2014.

[Hungr, O.: A review of landslide hazard and risk assessment methodology, in *Landslides and engineered slopes. Experience, theory and practice*, edited by: Aversa, S., Cascini, L., Picarelli, L., and Scavia, C., CRC Press, Boca Raton, FL, pp. 3-27 pp., 2018.](#)

Jin, S, Yang L, Danielson P, Homer C, Fry J, and Xian, G.: A comprehensive change detection method for updating the National Land Cover Database to circa 2011, *Remote Sens. Environ.*, 132: 159-175, 2013.

Kelsey, H.M.: Formation of inner gorges, *Catena*, 1 5: 433-458, 1988.

Kirschbaum, D.B., Adler, R., Hong, Y., Kumar, S., Peters-Lidard, C., and Lerner-Lam, A.: Advances in landslide nowcasting: evaluation of global and regional modeling approach. *Environ. Earth. Sci.*, 66: 1683-1696, 2012.

LaHusen, S. R., Duvall, A. R., Booth, A. M., and Montgomery, D. R.: Surface roughness dating of long-runout landslides near Oso, Washington (USA), reveals persistent postglacial hillslope instability. *Geology*, 44(2): 111-114, 2016.

Lee S., Pradhan, B.: Landslide hazard mapping at Selangor, Malaysia using frequency ratio and logistic regression models. *Landslides*, 4:33-41, 2007.

Lee, S., Ryu J. H., Kim, I. S.: Landslide susceptibility analysis and its verification using likelihood ratio, logistic regression, and artificial neural network models: Case study of Youngin, Korea. *Landslides*, 4:327–338, 2007.

Lepore, C., Kamal, S. A., Shanahan, P., and Bras, R. L.: Rainfall-induced landslide susceptibility zonation of Puerto Rico. *Environ. Earth Sci.*, 66(6): 1667-1681, 2012.

[Liang, X., Lettenmaier, D. P., Wood, E. F., and Burges, S. J.: A simple hydrologically based model of land surface water and energy fluxes for GSMS, J. Geophys. Res., 99, 14415–14428, 1994.](#)

Mancini, F., Ceppi, C., and Ritrovato, G.: GIS and statistical analysis for landslide susceptibility mapping in the Daunia area, Italy, *Nat. Hazard. Earth Sys.*, 10(9): 1851, 2010.

May, C.L., Pryor, B., Lisle, T.E., Lang, M.: Coupling hydrodynamic modeling and empirical measures of bed mobility to predict the risk of scour and fill of salmon redds in a large regulated river. *Water Resour. Res.* 45: W05402, 2009.

Megahan, W.F., Day, N.F., and Bliss, T. M.: Landslide occurrence in the western and central Northern Rocky Mountain physiographic province in Idaho, in *Forest Soils and Land Use: Proceedings of the Fifth North American Forest Soils Conference*, edited by: Youngberg, C.T., CSU, Ft. Collins, CO, 116-139 pp., 1978.

Miller, D. J., and Burnett, K. M.: Effects of forest cover, topography, and sampling extent on the measured density of shallow, translational landslides: *Water Resour. Res.*, v. 43, no. W03433, 2007.

Montgomery, D. R.: Road surface drainage, channel initiation, and slope instability. *Water Resour. Res.*, 30(6): 1925-1932, 1994.

Montgomery, D.R.: Slope distributions, threshold hillslopes, and steady-state topography. *Am. J. Sci.*, 301(4-5): 432-454, 2001.

Mustoe, G. E., and Leopold, E. B.: Paleobotanical evidence for the post-Miocene uplift of the Cascade Range. *Can. J. Earth Sci.*, 51(8): 809-824, 2014.

O'loughlin, E. M.: Prediction of surface saturation zones in natural catchments by topographic analysis. *Water Resour. Res.*, 22(5): 794-804, 1986.

Pachauri, A. K., and Pant, M.: Landslide hazard mapping based on geological attributes. *Eng. Geol.*, 32(1-2), 81-100, 1992.

Pelto M. S., and Riedel, J.: Spatial and temporal variations in annual balance of North Cascade glaciers, Washington 1984–2000. *Hydrol. Process.*, 15: 3461–3472, 2001.

Pollock, M. M.: Biodiversity, in: *River Ecology and Management: Lessons From the Pacific Coastal Ecoregion*, edited by: Naiman, R. J., and Bilby, R. E., Springer-Verlag, New York. 430–452 pp., 1998.

Poulos, M. J., Pierce, J. L., Flores, A. N., and Benner, S. G.: Hillslope asymmetry maps reveal widespread, multi-scale organization, *Geophys. Res. Lett.*, 39, L06406, doi:10.1029/2012GL051283, 2012.

[Reichenbach, P., Rossi, M., Malamud, B. D., Mihir, M., and Guzzetti, F.: A review of statistically-based landslide susceptibility models. Earth-Science Reviews, 180, 60-91, 2018.](#)

Riedel, J., Dorsch, S., and Wenger, J.: Geomorphology of the Stehekin River watershed: Landform mapping at North Cascades National Park Service Complex, Washington. *Natural Resource Technical Report NPS/NCCN/NRTR—2012/566*. National Park Service, Fort Collins, Colorado, 90 pp., 2012.

Riedel, J. L., Haugerud, R. A., and Clague, J. J.: Geomorphology of a Cordilleran Ice Sheet drainage network through breached divides in the North Cascades Mountains of Washington and British Columbia. *Geomorphology*, 91(1-2), 1-18, 2007.

Riedel, J., and Probala, J.: Mapping ecosystems at the landform scale in Washington state, *Park Science*, 23-2: 37-42, 2005.

Roering, J. J., Schmidt, K. M., Stock, J. D., Dietrich, W. E., and Montgomery, D. R.: Shallow landsliding, root reinforcement, and the spatial distribution of trees in the Oregon Coast Range, *Can. Geotech. J.*, 40, 237–253, 2003.

Roe, G.H.: Orographic Precipitation. *Annu. Rev. Earth Planet. Sci.*, 33:645–71, 2005.

Sidle, R.C., and Ochiai, H.: Landslides: processes, prediction, and land use, Water Resources Monogram 18, American Geophysical Union, Washington DC, 2006.

Strauch, R., Istanbulluoglu, E., Nudurupati, S. S., Bandaragoda, C., Gasparini, N. M., and Tucker, G. E.: A hydro-climatological approach to predicting regional landslide probability using Landlab, *Earth Surf. Dynam.*, 6(1), 49-75. <https://doi.org/10.5194/esurf-6-49-2018>, 2018.

Swanson, F. J., and Dyrness, C. T.: Impact of clear-cutting and road construction on soil erosion by landslides in the western Cascade Range, Oregon, *Geology*, 3: 393-396, 1975.

[Tabor, R.W., and Haugerud, R.A.: Geology of the North Cascades: a mountain mosaic. The Mountaineers Books, Seattle, WA, 1999.](#)

Taylor, F.A., and Brabb, E.-E.: Map showing landslides in California that have caused fatalities or at least \$1,000,000 in damages from 1906 to 1984: U.S. Geological Survey Miscellaneous Field Studies Map, MF- 1867, scale: 1:1,000,000, 1986.

United States Department of the Interior, National Park Service (DOI-NPS): Foundation Document, North Cascades National Park Complex, Washington. Available from: https://www.nps.gov/noca/learn/management/upload/North-Cascades-NP-Complex-Foundation-Document_small.pdf, last accessed: 23 January 2017, 2012.

United States Geologic Survey (USGS): National Elevation Data last modified March 6, 2014, National Map Viewer, last accessed: 24 November 2014, 2014a.

USGS: National Land Cover Data (NLCD) version Marched 31, 2014, National Map Viewer, last accessed: 25 November 2014, 2014b.

Van Westen, C.J., Van Asch, T.W., and Soeters, R.: Landslide hazard and risk zonation—why is it still so difficult? *B. Eng. Geol. Environ.*, 65(2): 167-184, 2006.

Wartman, J., Montgomery, D.R., Anderson, S.A., Keaton, J.R., Benoît, J., dela Chapelle, J., and Gilbert, R. (2016).: The 22 March 2014 Oso landslide, Washington, USA. *Geomorphology*, 253: 275-288, 2016.

Washington State Department of Natural Resources (WADNR).: Geologic_unit_poly_100k. Vector digital data, published June 2010. Division of Geology and Earth Resources, Olympia, WA, last accessed: March 27, 2014, 2014.

Wooten, R. M., Witt, A. C., Miniat, C. F., Hales, T. C., and Aldred, J. L.: Frequency and magnitude of selected historical landslide events in the southern Appalachian Highlands of North Carolina and Virginia: relationships to rainfall, geological and ecohydrological controls, and effects, in: *Natural Disturbances and Historic Range of Variation*, edited by: Greenberg, C. H., and Collins, B. S., Springer International Publishing, Switzerland, 203-262 pp., DOI 10.1007/978-3-319-21527-3, 2016.

Wu, Z., Wu, Y., Yang, Y., Chen, F., Zhang, N., Ke, Y., and Li, W.: A comparative study on the landslide susceptibility mapping using logistic regression and statistical index models. *Arab. J. Geosci.*, 10(8), 187, 2017.

Referee #1 comment response by authors

No.	Comment	Response
1	Why an independent training and testing dataset was not used for this approach. This is typical practice and it would be more robust if there was a separate validation dataset.	We did not perform a formal “validation” study. Instead, the improvements gained by the proposed methods in predicting landslide probability was obtained by a comparative ROC analysis. The focus of the study was to determine if an empirical-based model of landslide hazard could be used to improve an existing physically-based model for shallow landslide probability. A major reason for not separating the data to training and validation was that the performance of the statistical model improves with the size of the observational data used to train the model. The idea is to capture more spatial variability and geologic controls on observed landslides by using all the data we obtained for this region. Validation using ROC rather than training and testing datasets was used to assess this as has been used in similar studies (e.g., Kirschbaum et. al 2012). Future research could carry out validation approaches such as the training and testing approach suggested by the referee. This will be made more clear in the manuscript and suggested for future studies. Added sentence to last paragraphs of Introduction (pg. 4) and Results (pg. 29).
2	Provide a brief discussion on the accuracy and comprehensiveness of landslide inventories with respect to representative landslides over this region	The empirical data on landslides was obtained from a series of reports published by the National Park Service (Riedel and Probala, 2005). This comprehensive inventory across the 684,000 acre national park was conducted at 1:24,000 scale and based on 10 m DEMs, a series of large scale stereo air photographs taken since the 1960s, field verification, and from Lidar in a few basins. Where areas were mapped by traditional methods, and Lidar later became available, the original approach captured most (~75%) of the landslides. Dense vegetation cover and a lack of access also limited

		identification of some existing landslides. Larger, more recent debris avalanches that left large deposits on the valley floor were more easily recognized and mapped. Presence of observable landslide features were part of the mapping criteria, rather than mapping topographic imprint of landslides (e.g., Strauch et al., 2018). Ancient landslides that occurred before the last glacial period 16,000 years ago were generally not mapped because their deposits were buried or reworked by subsequent continental glaciation. This text will be incorporated into the revised paper. See additional text above Table 2 on pg. 13.
3	Discuss relevance of the methodologies for other regions.	See response to comment #5.
4	From the maps in 8e and f it is clear that accurately characterizing the entire landslide using the current methodologies is challenging. Can the authors comment a bit more on how this may be improved with differentiating source area from possibly considering a runout model to develop probabilistic estimates of runout?	Maps in 8e and 8f show the probability of initiation of slope failures, only applicable for slopes steeper than half of the internal friction angle of soils, which is the failure criterion for saturated soils. These maps reflect probability of landslide initiation, which was the focus of the integrated model as described in Section 2.2. The model test using the ROC analysis in Fig. 10 is also conducted only for source areas. Thus, the current integrated methodology is not developed for characterizing the probability of an entire landslide. As the occurrence of runout is conditioned on the failure of source areas, these two models can be developed separately and linked for applications. Differentiating the source area from the transport and deposition portions of landslides, in an inventory could improve the characterization of site features and conditions conducive to failure initiation, transport and deposition. In our paper, only source areas are identified by the integrated model; transport and depositional zones are not addressed as the physical model doesn't apply. We agree with the reviewer that developing a probabilistic runout component would improve the prediction of hazards from the entire landslide disturbances. There could be several different ways of developing a runout model. We could map runout zones of landslides from

		<p>our inventory and train a rule-based runout model, or develop a purely statistical model based on the occurrence of runout in relation to geologic and topographic attributes. If well-developed and tested, combining a runout model with the initiation methodology we proposed in this paper should improve prediction of hazards from entire landslides.</p> <p>Additional text will be included in the manuscript to suggest these model advancements. See additional text in last paragraph of Conclusions (pg. 30).</p>
5	<p>It would be helpful to have a bit more discussion on the applicability of these methods to other regions, including the size of the region over which this methodology could be applied and other considerations.</p>	<p>The applicability of this approach to characterize shallow landslides hazard is limited by the quality of the site-specific data on soils and vegetation, extent of hydrologic modeling, as well as the comprehensiveness of the landslide inventory. Accurate data for environmental variables such as rock, soils, and vegetation would be as important as comprehensive landslide data as our method relates landslide risk to the environmental variables. The spatial scale of data is another issue we have not studied yet with this method. Larger data sets would profoundly improve predictions, however they could also increase uncertainty of predictions. We argue that this method should be used along with other mapping methods and its performance should be compared against other methods using ROC analysis or other tests. It could potentially be applied over large areas, even continental scales, if these data are available, complete, and validated. The design of the methodology described and demonstrated in this paper allows broad application and is not limited to use at the specific location within Washington, U.S.A. Advancements in surface terrain delineation and in distributed hydrologic modeling specifically contribute to the broad applicability of this approach. We will add additional text to capture these applications. See additional text in last paragraph of Conclusions (pg. 30).</p>
6	Specific comments on manuscript	<p>Suggested edits and clarifications called out within the draft manuscript are helpful for</p>

		improving the writing and clarity of the findings. For example, additional explanation on the association with developed landscape is provided in Section 3.1 (pg. 17) as well as additional thoughts on the importance of mapping accuracy in Conclusions (pg. 30). Suggested figure improvements were also appreciated and are updated in the final manuscript.
--	--	---

Referee #2

No.	Comment	Response
1	The term “process-based method” should be changed in the more correct “physically-based model” to define deterministic methods of assessment of slope stability. This correction has to be inserted throughout all the paper.	Agreed, changes made throughout paper.
2	Several examples of both data-driven techniques and physically-based models, and related references, could be add in the Introduction section.	We provided literature review in a separate data-driven and physically-based model review paragraphs in the Introduction of the paper. If the referee knows of relevant papers to cite in our paper that we missed and shares them with us, we would consider including them in the Introduction of our paper and discuss their key aspects.
3	I disagree with the choice of the Authors of considering the entire landslides bodies, both triggering and accumulation zones, as predictor variable of the data-driven method. Landslides runout and accumulation zone are related to other predisposing factors than the ones influencing the the landslides triggering. Instead, I know that the approach of using the entire landslide body in a data-driven approach is very common in the literature. Thus, I suggest to add the reasons why the Authors have chosen this approach and to discuss about	As the referee notes, considering the entire mapped landslide is a common approach in data-driven hazard identification. We too agree with the limitation of this approach. Thus, we developed two other methods that used landslide source areas and a single landslide type to study how the first could improve a physically-based model and to allow comparisons with these previous studies. Often, only the entire landslide or portions of the landslide are mapped as part of an inventory, and many inventories lack information on types of landslides. Thus, we wanted to explore and demonstrate the differences in the site characteristics associated with these various types of datasets. This type of

	the potential limits of this choice.	analysis can provide insights into the value of more specific inventories, depending on the goals of the hazard identification study. Some studies are content with identifying landslide prone areas regardless of the type of landslide or landslide feature. However, our analysis demonstrates the variability in results, depending on the landslide dataset used, given the same site attributes. The limitations with these datasets and resulting hazard maps, relate to the objectives of the study and intended use. For example, using all landslide types may highlight general areas where landslide activity is possible, but it does a poor job at identifying where landslide may initiate. More explanation of these important choices and limitations will be added to the Methodology (pg. 7) and Conclusion (pg. 30) in the manuscript.
4	It is necessary to describe the main features and the main outputs of the Landlab model considered for the implementation of the physically-based approach. In particular, how the rainfall features are inserted and considered by this model?	In this paper we directly use predicted landslide probability from a physically-based shallow landslide model reported in Strauch et al. (2018). The landslide model developed in Landlab has been detailed extensively in Strauch et al. (2018). However, we agree that additional detail on the main features and outputs could be added to the text in Sect. 2.2 Model Integration (pg. 7-8). Precipitation is considered in the landslide model through its use as input to a macro-scale hydrology model, Variable Infiltration Capacity model. This model produces a spatially distributed recharge field which is used to form subsurface flow in Landlab (see pg. 8). A probability distribution of recharge is used to determine soil relative wetness within Monte Carlo simulations of factor-of-safety.
5	A more detailed description of the bedrock geological features and on the main properties of the soil type are required in the presentation of the study area.	The bedrock geology in North Cascades National Park is dominated by gneiss and granite, with lower grade metamorphic rocks schist and phyllite on the western edge of the park, and Mesozoic sedimentary rocks on the eastern flank (Tabor and Haugerud, 1999). Placement of granite at depth along faults led to hydrothermal alteration of some overlying rocks, and the clustering of large landslides. Soils in the park are generally coarse-grained

		and relatively young due to active slope processes, but soil age, thickness and distribution are highly variable. Soils formed in glacial deposits from the last ice age are also widespread, and many soils are classified based on the amount of volcanic ash they contain. This detail will be added to the study area description on pg. 11.
6	Considering in the same inventory rockfalls/topple and debris flows/avalanches is not really correct. These phenomena are characterized by different kinematic behaviors their predisposing factors can be different. Even if the combined probability model between data-driven and physically-based approaches have been obtained only taking into account for the source areas of debris flows/avalanches, I advise to add an explanation of why you consider different typologies of landslides in the same inventory of your study area.	Please see response to comment #3.
7	For a further validation of the data-driven model, it could be useful calculating a statistical index such as the Area Under ROC Curve or the values of False Positives/True Positives. This would strengthen the reliability of the proposed model.	We included the physically-based model and the integrated model in Fig. 10b. Our intent with the ROC curves was to see if the empirical information could improve the physically-based model results by providing some unknown information missing from the infinite slope model. An ROC curve from the data-driven model would show a well performing model by definition because it is derived from the observations used to develop the susceptibility index or probability and the AUC for the empirical models alone would support the model performance.
8	It could be useful presenting also the results of the application of the physically-based probabilistic model implemented in the study area and its validation.	This information is provided in an earlier study by Strauch et al. (2018) and is not repeated here for the sake of brevity.
9	Why did the Authors choose those ranges of probability to consider a slope as relatively stable (< 0.1) or	The terms relative stable and highly unstable were terms chosen by the authors to identify where the cumulative distribution curve

	highly unstable (> 0.9). Several Authors identified other ranges for the classification of the probability distribution. Please, discuss about this aspect.	generally shifts direction. In between these probabilities, a small portion of the landscape is modeled to have a wide range of failure potential. We removed the labels from the figures and instead, added the corresponding return periods of 10 years and 1.1 years to provide a sense of the hazard distribution, similar to the plotting used in Strauch et al. (2018). Additionally, we modified the text to further clarify interpretation of the figure on pg 26 and 29.
10	It is necessary adding a section where the Authors will discuss about the main advantages and the limitations of their proposed approach, in particular compared with the typical methodologies used for the assessment of landslides susceptibility or hazard.	Many articles have described the advantages and disadvantages to data-driven and physically-based models (e.g., Ercanoglu and Sonmez, 2019; Reichenback, et al., 2018; Hungr, 2018; Aleotti and Chowdhury, 1999). Our approach attempts to benefit from the strengths of both traditional modeling methods. While empirical models validate well with given mapped landslides, they lack a mechanistic explanation for the susceptibility level. Parsimonious physical models predict failure based on forces within the soil, but they may miss properties demonstrated by failure or lack of failure on the landscape. Our approach is limited to areas where landslides have been mapped. Additional text and references will be added to explain the main advantages and limitations of our integrated approach (see pgs. 3 and 30).